Distributed force feedback-based reflex with online learning for adaptive quadruped motor control

Tao Sun[a,b], Zhendong Dai[a], Poramate Manoonpong[a,b,*]

[a] *Institute of Bio-inspired Structure and Surface Engineering, College of Mechanical and Electrical Engineering, Nanjing University of Aeronautics and Astronautics, Nanjing, China*
[b] *Embodied AI & Neurobotics Lab, SDU Biorobotics, the Mærsk Mc-Kinney Møller Institute, the University of Southern Denmark, Odense M, Denmark*

Abstract

Biological motor control mechanisms, such as central pattern generators (CPGs), sensory feedback, reflexes, and motor learning, play a crucial role in the adaptive locomotion of animals. However, the interaction and integration among these mechanisms for generating efficient adaptive locomotion of legged robots to deal with diverse terrains have not yet been fully realized. One issue is to achieve adaptive motor control for fast postural adaptation on various terrains. To address this issue, this study proposes a novel distributed force feedback-based reflex with online learning (DFRL). It integrates force sensory feedback, reflex, and learning to cooperate with CPGs for producing adaptive motor commands. The DFRL is based on a simple neural network with plastic synapses modulated online by a fast dual integral learner (DIL). Experimental results on different quadruped robots show that the DFRL can: 1) automatically and quickly adapt the CPG patterns (motor commands) to the robots, enabling them to perform appropriate body posture during locomotion, and 2) enable the robots to effectively accommodate various slope terrains including steep ones. Consequently, the robots driven by the DFRL can successfully perform efficient adaptive locomotion to deal with complex terrains with diverse slopes.

*Corresponding author
Email addresses: s.tao@nuaa.edu.cn (Tao Sun), zddai@nuaa.edu.cn (Zhendong Dai), poma@nuaa.edu.cn (Poramate Manoonpong)

Keywords: Reflexes, CPGs, Motor learning, Offset adaptation, Slope terrains, Quadruped robots.

1. Introduction

Animals show elegant locomotion with impressive adaptation, and this has been the primary source of inspiration for developing advanced robot locomotion control [1]. To date, certain quadruped robots (such as SpotMimi [2], Laikago[1], ANYmal [3], MIT cheetah [4], LittleDog [5], and HyQ2Max [6]) have demonstrated excellent locomotion behaviors. However, their controllers are based on classical engineering control techniques (e.g., whole body control [7], inverse dynamic model-based control [5], optimization-based control [8], and nonlinear model predictive control (MPC) [9]) which are highly reliant on precise/specific dynamic or kinematic robot models and their environments. Thus, their control performance is highly dependent on the quality of the model. These techniques also require extensive knowledge and intensive computation for control parameter optimization. Moreover, it is still difficult to relate the robot techniques to their biological counterparts and understand the biological locomotion control mechanisms involved.

Therefore, the development of genuine bio-inspired control without reliance on robot and environment models not only has promising potential for successfully mimicking dexterous animal-like locomotion with computational efficiency, but also provides a basis for validating a hypothesis on biological investigation [10].

Central pattern generators (CPGs) for generating rhythmic synchronized patterns and reflexes with sensory feedback for realizing adaptation of the patterns play a crucial role in the control of animal locomotion [11, 12, 13, 14, 15]. However, the interaction and integration among these mechanisms for generating efficient adaptive locomotion on complex terrains still remain under

[1] https://www.unitree.cc

investigation in robot locomotion [11, 16, 17, 10]. Although certain existing CPGs-based controls include CPG phase adaptation for generating adaptive gaits [18, 19] and CPG frequency adaptation for generating efficient stepping frequency [20], CPG offset adaptation for obtaining adaptive body posture corresponding to diverse terrains (Fig. 1) has only been partially investigated, as described below.

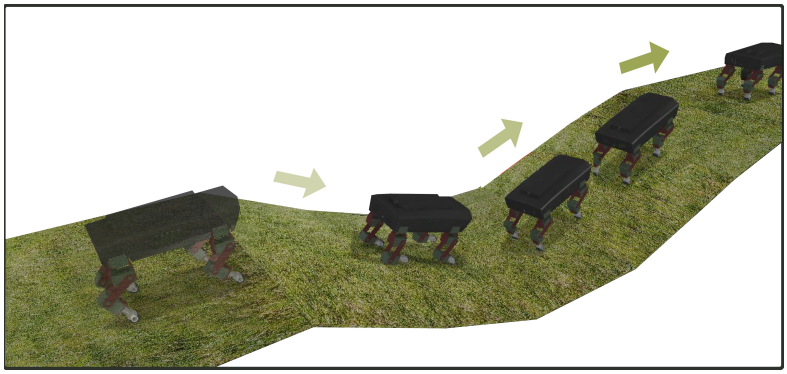

Figure 1: A quadruped robot adaptively trots on a complex terrain with multiple slopes. It is driven by distributed force feedback-based reflex with online learning.

Fukuoka et al. presented a groundbreaking study on bio-inspired control for adaptive quadruped walking on irregular terrains. The control is composed of four connected Matsuoka CPGs [21] with sensory feedback to form basic rhythmic patterns and multiple reflexes (i.e., vestibular reflex, flexor reflex, stepping reflex, sideways and corrective stepping reflexes, and crossed flexor reflex). This results in body posture adaptation [17]. However, the reflexes are predefined using several hand-tuned parameters for specific platforms. Such a vestibular reflex [17] (or postural reflex) has also been used together with various CPG models for generating adaptive body posture, thus enabling the robot to walk on different slope terrains [22, 23, 24, 25, 26, 27, 28]. Nonetheless, all these cases are limited to low slopes (less than 20°, see Table 1). This is because the vestibular reflex utilizes only body posture information (i.e., body orientation) to keep it in parallel to the ground (known as telescoping strut strategy in biomechanics [29]). The robot can then obtain a balance by almost fully ex-

tending or flexing its legs, thereby leading to the joint movement near to their singular configuration or joint limits [30], particularly on steep slopes (e.g., 30°). Although the traditional vestibular reflex can endow the CPGs with adaptive offsets for balancing body posture, these rely on elaborately predefined control parameters, and still have limited ability on high and complex slope terrains (Table 1) (see also the Experiments and Results section).

Instead of the vestibular/postural reflex that requires elaborately design with manual control parameter tuning, machine learning, especially reinforcement learning (RL), has been increasingly applied for automatic control parameter tuning. This is because it is not only model free, but also has high potential to generate robot agility, complex motor skills, and adaptability to various environments [31, 32, 33, 34, 35]. For instance, Hwangbo et al. have proposed an RL-based method for training a neural network policy in simulation and transferred it to the quadruped robot ANYmal that can perform agile and dynamic motor skills [32]. To avoid long training sessions (e.g., 9 days for training a normal locomotion on a floor) due to the structural complexity of the neural network [32], Thor et al. have recently presented a novel control framework which transfers CPG signals into desired joint motor commands for robot locomotion via radial basis function (RBF) network with a simplified structure [34]. The network was trained by black box optimization (BBO, a variant of the RL-based policy improvement with Path Integrals (PI2)) to generate the desired commands. Although the framework has ability to also implicitly realize adaptive offsets for CPG signals, it still requires several training sessions (up to 100 minutes). Such machine learning techniques, while impressive in their own right, typically need 1) a number of training sessions from several minutes to days and 2) careful objective function training scenario designs. Furthermore, they might fail to deal with situations which have not been trained before (generalization issue).

To overcome the limitations of the aforementioned control techniques (classical engineering, bio-inspired CPGs with reflexes, and (data-driven) machine learning), we present a novel distributed force feedback-based reflex with on-

line learning (DFRL) for fast offset adaptation of a CPG. The DFRL utilizes the distribution of the ground reaction forces (GRFs), acting on robot feet, as sensory feedback. It can stimulate a response modulation on the CPG offsets in real time for posture adjustment and balance. This strategy is known in biomechanics as the lever mechanics [29].

The distributed force feedback-based (DFFB) reflex is implemented through a simple recurrent neural network organized in three layers. The key synaptic weights in the network are plastic are adapted by a fast online learning mechanism, called dual integral learners (DIL) [20] . The employed learning mechanism endows the reflex with fast adaptation capability due to the induced synaptic plasticity of the reflex neural network. Therefore, the DFRL has several advantages compared to the traditional vestibular reflex [23, 24, 25, 26, 17, 27], including online learning for fast automatic control parameter tuning, posture self-stabilization on various slope terrains, and the capability to handle steep and complex slope terrains. Since implementation of the DIL prevents manual control parameter tuning for a specific robot platform, the DFRL can be simply applied to other robot platforms. To access the performance of the DFRL, we integrated it with simple CPGs-based control. This results in adaptive quadruped motor control (Section 2). A comparison with the traditional vestibular reflex shows the superior performance of the DFRL for adaptive quadruped locomotion (Section 3). The discussion and conclusion are presented in Sections 4 and 5, respectively.

Taken together, the main contributions of this work are: 1) a novel bio-inspired reflex mechanism with fast online learning, which endows CPGs-based control with an offset adaptation function, for adaptive body posture corresponding to diverse slopes; 2) a demonstration involving quadruped robots with the proposed reflex for adaptive body posture to deal with ascending and descending steep slopes (i.e., $\pm 35^\circ$ for a small sized robot and 50° and -45° for a larger one) as well as a complex terrain with multiple slopes using a trot gait (see Fig. 1); 3) a comparison of the performance between the traditional vestibular reflex (using the telescoping strut strategy) and the proposed DFRL (using

Table 1: The maximum slope to which robots can adapt based on vestibular reflex modulation.

Works	Year of publication	Max. slope [degree]
Xiuli Zhang et. al. [24]	2008	Around 11.2
Mostafa Ajallooeian et. al. [26]	2013	11.85
Duc Trong Tran et. al. [22]	2014	Around 11
Chengju Liu et. al. [23]	2018	Around 12

the lever mechanics strategy) for adaptive quadruped locomotion on various slopes; 4) analysis of the body posture adaptation mechanism. To this end, the proposed DFRL based on biological mechanisms is characterized by the independence of specific robots and CPGs-based control. It provides a generic offset adaptation method with the possible option for integration and interaction of CPGs, sensory feedback, reflexes, and motor learning.

2. Adaptive quadruped motor control

In this section, we introduce an adaptive quadruped motor control based on biological mechanisms: CPGs, sensory feedback, reflex, and online (motor) learning. The control is bio-inspired, model-free, and straightforward with fast control parameter adaptation. It is derived from an integration of CPGs-based control and the DFRL (see Fig. 2). More specifically, the CPGs-based control, realized by four identical coupled neural oscillators, can spontaneously produce synchronized periodic signals. These signals are transferred to drive joint movements through motor neurons (MNs). The MNs (and CPGs) offsets can be quickly adjusted by the DFRL online for body balance and stable locomotion depending on the GRFs distribution. The DFRL is realized by the DFFB reflex and the DIL. In this way, the adaptive motor control can enable quadruped robots to autonomously adapt their body posture to various complex terrains (see Fig. 1).

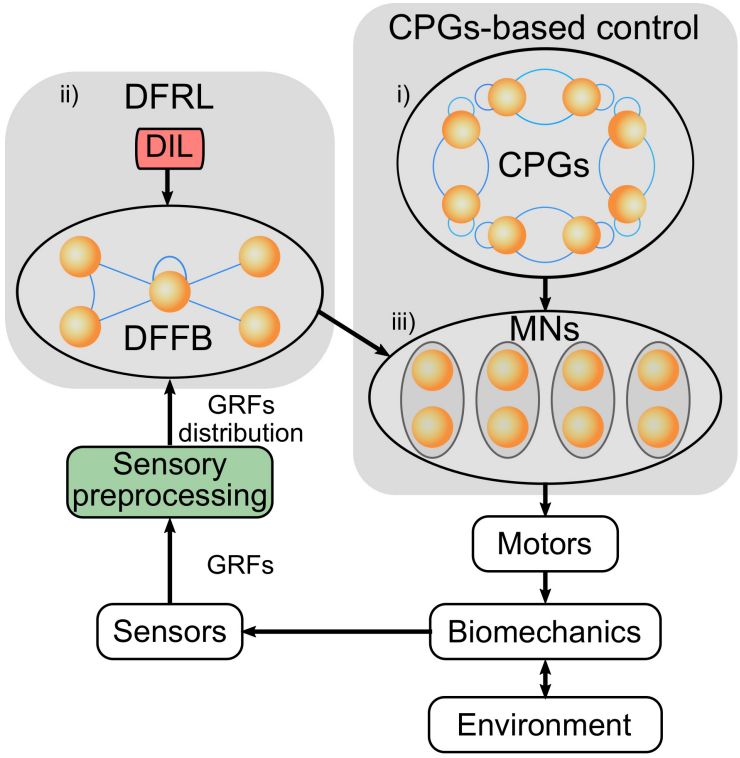

Figure 2: Schematic diagram of the adaptive quadruped motor control. It has i) a CPGs network for generating rhythmic commands, ii) the DFRL, including the DFFB reflex and DIL, using GRFs information for CPG offset adaptation, and iii) the MNs for integrating and transferring the adaptive commands from the CPGs and DFFB reflex to drive robot leg-joint movements.

2.1. Central pattern generators (CPGs)-based control

Here, we employ concise and straightforward neural CPGs-based control involving two basic modules: CPGs and MNs (Fig. 2). The CPGs are used to generate rhythmic signals for robot's joints. Here they are implemented as four coupled neural SO(2) CPGs [36] (see Fig. 3 (a)). Each SO(2)-based CPG, acting as an abstract neural oscillator, is a recurrent neural network (Fig. 3 (b)). It consists of two fully-connected standard additive time-discrete neurons N1 and N2, both using a sigmoid transfer function. The two neurons N1 and N2 output two signals o_1 and o_2, respectively. And there is a stable phase shift $\pi/2$

between them for realizing intralimb coordination of a leg [19]. The connections among CPGs determine the interlimb coordination of all legs. The MNs are used to transfer the CPG outputs into the desired joint movement commands. Their transfer function are also a sigmoid. The sigmoid function enables the MNs to capture the main features of the CPG outputs, such as frequency, waveform (i.e., duration of the ascending and descending in a cycle), phase relationships among the outputs, and offset. The MN output amplitudes can be scaled to meet the joint movement range through the synaptic weights projecting from the CPGs to MNs. As a result, the robot feet will show alternative stance and swing motion states when the robot is balanced at the lift/touch moment (Fig. 3 (d)). The neural model of each CPG is given as follows:

$$\mathbf{a}(n+1) = \mathbf{w} \cdot \mathbf{o}(n) + \mathbf{b} + \mathbf{g}(n), \tag{1}$$

$$\mathbf{o} = \tanh(\mathbf{a}), \tag{2}$$

where $\mathbf{a}, \mathbf{o}, \mathbf{b}$, and $\mathbf{g} \in \mathbb{R}^{2\times 4}$ represent the activities, outputs, biases, and gait term of the CPGs, respectively. $\mathbf{w} \in \mathbb{R}^{2\times 2}$ indicates the synaptic weights between the two neurons in each CPG network. $\mathbf{w}$ determines a phase relationship in the outputs o_1 and o_2 of a CPG, realizing the intralimb coordination of a leg, while $\mathbf{g}$ defines the interlimb coordination among all legs (i.e., all CPGs). In the following experiments, the bias, weights and gait term are as follows:

$$\mathbf{b} = \begin{pmatrix} 0.01 & 0.01 & 0.01 & 0.01 \\ 0.01 & 0.01 & 0.01 & 0.01 \end{pmatrix}, \tag{3}$$

$$\mathbf{w} = \begin{pmatrix} w_{11} & w_{12} \\ w_{21} & w_{22} \end{pmatrix} = \begin{pmatrix} 1.4 & 2.6 \\ -2.6 & 1.4 \end{pmatrix}, \tag{4}$$

$$\mathbf{g}_i^l(n) = \xi \sum_{k=1}^{4} \left(\sin\left(o_i^l(n) - o_i^k(n) - \Phi_{lk} \right) \right), \tag{5}$$

[2]Lilibot is our small-sized quadruped robot used in this study (see Fig. 7 and Appendix)
[3]Laikago is the large quadruped robot used in this study (see Fig. 7 and Appendix)

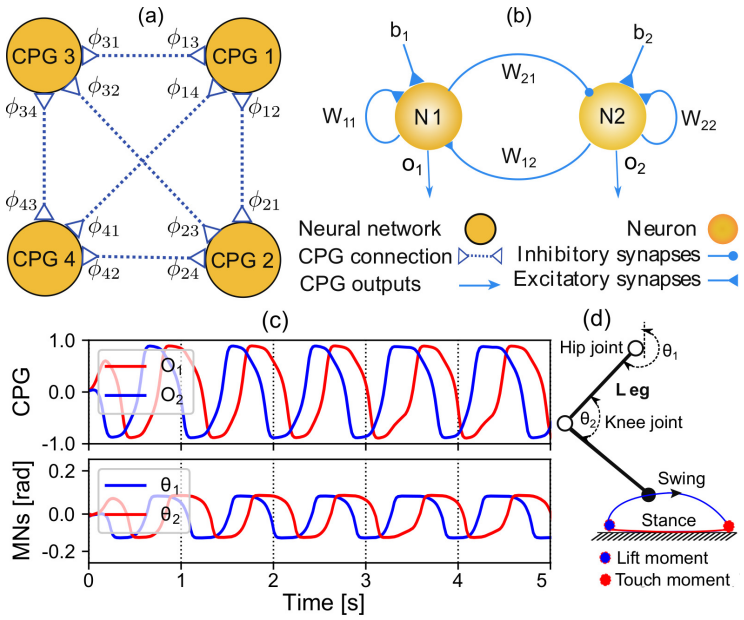

Figure 3: CPGs-based control. (a) Four identical SO(2)-based CPGs which are connected to each other to form periodic commands for interlimb coordination with specific phase relationships among four corresponding legs. (b) The recurrent neural network of an SO(2) CPG. It consists of two fully connected standard additive time-discrete neurons N1 and N2. They have two outputs o_1 and o_2 with a fixed phase shift $\pi/2$. (c) The outputs of the CPG and MNs of a leg. The MNs outputs θ_1 and θ_2 convey the frequency, waveform, phase, offset of the CPGs outputs o_1 and o_2 to the robot joints. The amplitudes of the MN outputs are scaled by synaptic weights projecting from the CPGs to MNs (e.g.., 0.16 for Lilibot[2] and 0.12 for Laikago[3]) to form a particular step length. (d) The foot trajectory formed under the MNs outputs. Ideally, the trajectory has four cyclic states: lift moment, touch moment, swing phase, and stance phase.

where $o_i^l(n)$ and $o_i^k(n)$ are the outputs of the ith neurons in the CPGs l and k. Φ_{lk} is the desired relative phase of the CPG k with respect to the CPG l. ξ is a communication gain which is empirically set to 0.01. For a trot gait, Φ_{lk} is defined as follows (Fig. 3 (a)):

$$\mathbf{\Phi} = \begin{pmatrix} \phi_{11} & \phi_{12} & \phi_{13} & \phi_{14} \\ \phi_{21} & \phi_{22} & \phi_{23} & \phi_{24} \\ \phi_{31} & \phi_{32} & \phi_{33} & \phi_{34} \\ \phi_{41} & \phi_{42} & \phi_{43} & \phi_{44} \end{pmatrix} = \begin{pmatrix} 0.0 & -\pi & -\pi & 0.0 \\ \pi & 0.0 & 0.0 & \pi \\ \pi & 0.0 & 0.0 & \pi \\ 0.0 & -\pi & -\pi & 0.0 \end{pmatrix}. \tag{6}$$

The parameter setups utilized here have been investigated in our previous study [37].

The MNs are defined as follows:

$$\boldsymbol{\theta} = tanh(\alpha \mathbf{o} + \boldsymbol{\beta}), \tag{7}$$

where $\mathbf{o}$, $\boldsymbol{\beta}$, and $\boldsymbol{\theta} \in \mathbb{R}^{2\times4}$. $\boldsymbol{\theta}$ is the joint command, $\mathbf{o}$ is the CPGs output, α represents the synaptic weight projecting from the CPGs and MNs. It can scale the command amplitude for appropriate robot joint ranges (e.g., 0.16 for Lilibot and 0.12 for Laikago). $\boldsymbol{\beta}$ indicates the command offset, and thereby determines the robot joint offsets so as to influence the robot posture. The automatic adjustment of $\boldsymbol{\beta}$ by the DFRL is elucidated in the following subsection.

2.2. Distributed force feedback-based reflex with online learning (DFRL)

The DFRL is realized by the DFFB reflex and the DIL (Fig. 2). The DFFB reflex is organized by a simple neural network with synaptic plasticity. The network can be triggered by the GRFs distribution while the network plastic synapse strengths can be online adapted by the DIL.

2.2.1. Distribution of ground reaction forces (GRFs)

The distribution of GRFs acting on the robot feet is proved to be an effective index of robot motion stability and efficiency [38, 39, 40]. Here, it is formulated as sensory feedback for stimulating the DFFB reflex to maintain locomotion

stability by adjusting CPG/joint offsets. This, of course, realizes the adaptability of CPG offsets. In the robot model illustrated in Fig. 4 (a), F_f and F_h represent the GRFs of the front and hind legs, respectively, while ma is the resultant force acting on the body in the sagittal plane, which points the zero moment point (ZMP) on the ground when robot locomotion is stable [41]. It should be noted that, each leg mass is neglected since it is light in comparison with the robot body weight. The ZMP position can be described by x_1 and x_2 in the sagittal plane, by which a stability index γ can be depicted as below.

$$\gamma = x_1/x_2, \tag{8}$$

where x_1 and x_2 are the distances between the footholds and ZMP (see Fig. 4 (a)). In addition, we can acquire the following equilibrium equation of the robot:

$$x_1 \cdot F_h = x_2 \cdot F_f. \tag{9}$$

Combining (8) and (9), γ can be conveniently online calculated using the GRFs signals measured by foot force sensors in Eq. (10).

$$\gamma = \begin{cases} F_f/F_h & F_h \neq 0 \\ 0 & F_h = 0 \end{cases}. \tag{10}$$

Therefore, the stability index can also be considered as a metric of the GRFs distribution. This is the base of the idea that the DFFB reflex can maintain locomotion stability using GRFs distribution as sensory feedback.

2.2.2. Distributed force feedback-based (DFFB) reflex

Intuitively, there are two fundamental and essential motion conditions for a stable trot gait of quadruped robots. Firstly, flight feet must be able to touch the ground in time to support the robot body for ensuring the regular alternation (touching condition). Secondly, the support feet must be able to lift to swing in time so as to make a step (lifting condition). The first condition can easily be realized by using either a high step frequency or small step length. In this work,

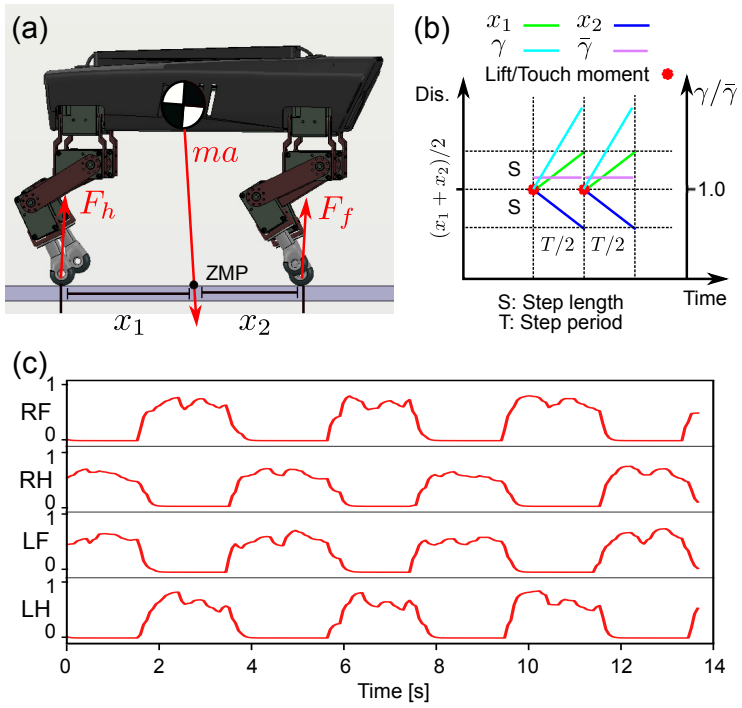

Figure 4: GRFs distribution. (a) Force balance of the quadruped robot at a moment when its feet touch the ground. (b) The ideal profile of the parameters x_1, x_2, γ, and $\bar{\gamma}$ during a step period while the robot stably trots forward, where x_1 increases while x_2 decreases in every half period. Thus, γ increases significantly from 1.0 at the lift/touch moment. $\bar{\gamma}$ (see Eq. (11)), obtained by smoothing γ, is a constant value greater than 1.0. (c) The filtered GRFs of four legs when a quadruped robot performs stable locomotion using a trot gait. RF, RH, LF, and LH are the right front, right hind, left front, and left hind legs, respectively.

we focus on the second condition to handle the more complex lifting condition (e.g., lifting when walking on a slope).

This will be performed by the proposed DFFB reflex mechanism since it can appropriately redistribute the GRFs on the stance feet by adjusting the body posture with respect to the ground, thereby allowing the support feet to lift as desired movement. The desired lifting movement results from the GRFs between the front and hind legs ideally being approximately equal at the lift moment ($n = n_0$) (see Fig. 4 (b)). This means that $F_f(n_0) = F_h(n_0)$, or $\gamma(n_0) = 1$ (Eq. (10)), where n_0 indicates the moment at which the stance and swing phases switch. As shown in Fig. 4 (b), the ideal profile of γ is reset to 1.0 at each lift/touch moment (n_0) during an ideal trot locomotion. However, γ increases significantly in each half step period after the lift/touch moment (n_0). This indicates that the trot gait is not statically stable. To avoid an unstable situation where the robot might fall down, the γ value should be reset in a timely manner.

However, in reality, it is difficult to precisely determine the touch moment (n_0) and promptly obtain $F_{f,h}(n_0)$ and $\gamma(n_0)$. Therefore, in practice, a smoothed GRFs distribution variable ($\bar{\gamma}$) is used for locomotion state estimation and sensory feedback for the DFFB reflex. $\bar{\gamma}$ implies the average value of γ during a certain periods (Eq. (11)). When a stable trot gait of quadruped robots emerges, the γ profile, determined by the specific step length (or joint movement range) and period, should be a constant pattern (Fig. 4 (b)). Thus, the corresponding $\bar{\gamma}$ should be a constant value. In the following robot experiments, the desired $\bar{\gamma}$ is around 1.1 when the robots stably trot, i.e., the joint movement ranges (determined by α, Eq. (7)) of Lilibot and Laikago are 0.16 rad and 0.12 rad, respectively, while their step periods are around 1.5 seconds.

2.2.3. Distributed force feedback-based reflex with online learning (DFRL) realization

As shown in Fig. 5, the DFRL consists of three sub-modules including 1) sensory preprocessing for properly computing GRFs distribution, 2) a neural

control network for implementing the DFFB reflex to transfer sensory stimulation to motor outputs, and 3) a dual integral learner (DIL) for online adapting the synaptic strengths of the reflex neural network.

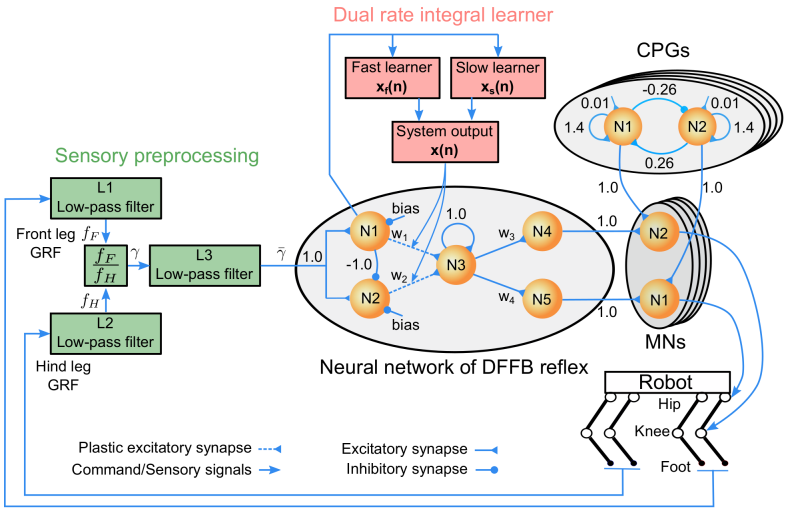

Figure 5: Schematics of the DFRL. The DFFB reflex neural network, organized by five connected neurons (N1, N2, N3, N4, and N5), autonomously adjusts the CPGs command offsets to stabilize locomotion. Two plastic synapses (w_1 and w_2) of the network are online modulated by the DIL. The biases of N1 and N2 in the network represent the negative desired smoothed GRFs distribution ($\bar{\gamma}^d$). In the following experiments, the they are set to -1.1 depending on the particular step length and period. w_3 and w_4 indicate the synapses to output neurons N4 and N5, respectively. Normally, w_3 is about twice w_4 (i.e., w_3=2.0, w_4=1.0). The sensory preprocessing calculates γ using the front and hind GRFs signals filtered by two IIR low-pass filters (L1 and L2 low-pass filers), and then smooths γ using a moving average filter (L3 low-pass filter) to acquire an actual smoothed $\bar{\gamma}^a$ for transmission to the reflex network.

The sensory preprocessing unit real-time calculates the distribution (γ) of the front and hind GRFs (F_f and F_h) that are smoothed by two digital low-pass single-pole infinite impulse response (IIR) filters. The GRFs distribution (γ) is then further processed by a two-layers moving average filter defined by Eq. (11)

to obtain a smoothed GRFs distribution ($\bar{\gamma}$).

$$\begin{aligned} \gamma(n)_{temp} &= \frac{1}{N} \sum_{k=n-N}^{n} \gamma(k), \\ \bar{\gamma}(n) &= \frac{1}{0.5N} \sum_{k=n-0.5N}^{n} \gamma(k)_{temp}, \end{aligned} \tag{11}$$

where n and $N \in \mathbb{R}$. n indicates the current sample number. N represents the sample size of the filter. It was empirically set to 50 in the robot experiments here.

The DFFB reflex neural network employs the smoothed GRFs distribution ($\bar{\gamma}$) as its sensory input to trigger neural network activation. The composition of the neural network can be regarded as three layers with five standard additive time-discrete neurons whose transfer functions are linear (see Fig. 5). The input layer has two neurons (N1 and N2) for receiving GRFs distribution information. They are connected to a recurrent neuron (N3) of the hidden layer by plastic synapses (w_1 and w_2) for calculating reflex outputs. The output layer has two neurons (N4 and N5) for scaling the reflex outputs through synapses (w_3 and w_4). Afterward, the DFFB reflex N4 and N5 outputs (o_4^{dffb} and o_5^{dffb}) are transferred to N2 and N1 of the MNs. Thus, the inputs of the MNs result from the sum of the CPG and DFFB reflex outputs. Referring to Eq. (7), o_4^{dffb} and o_5^{dffb} are regarded as the joint command offsets ($\boldsymbol{\beta}$). It can be described as follows:

$$\begin{aligned} \beta_1 &= o_5^{dffb}, \\ \beta_2 &= o_4^{dffb}. \end{aligned} \tag{12}$$

Therefore, the DFFB reflex can automatically adjust the MN output offsets to sustain proper body posture in accordance with the GRFs distribution. As shown in Fig. 6 (a), the offsets (β_1 and β_2) of the corresponding MN outputs (θ_1 and θ_2) are online adjusted leading to the GRFs distribution ($\bar{\gamma}$) converging to a desired value (i.e., 1.1, Fig. 5).

In addition, the synaptic weights (w_1 and w_2) in the DFFB network, which

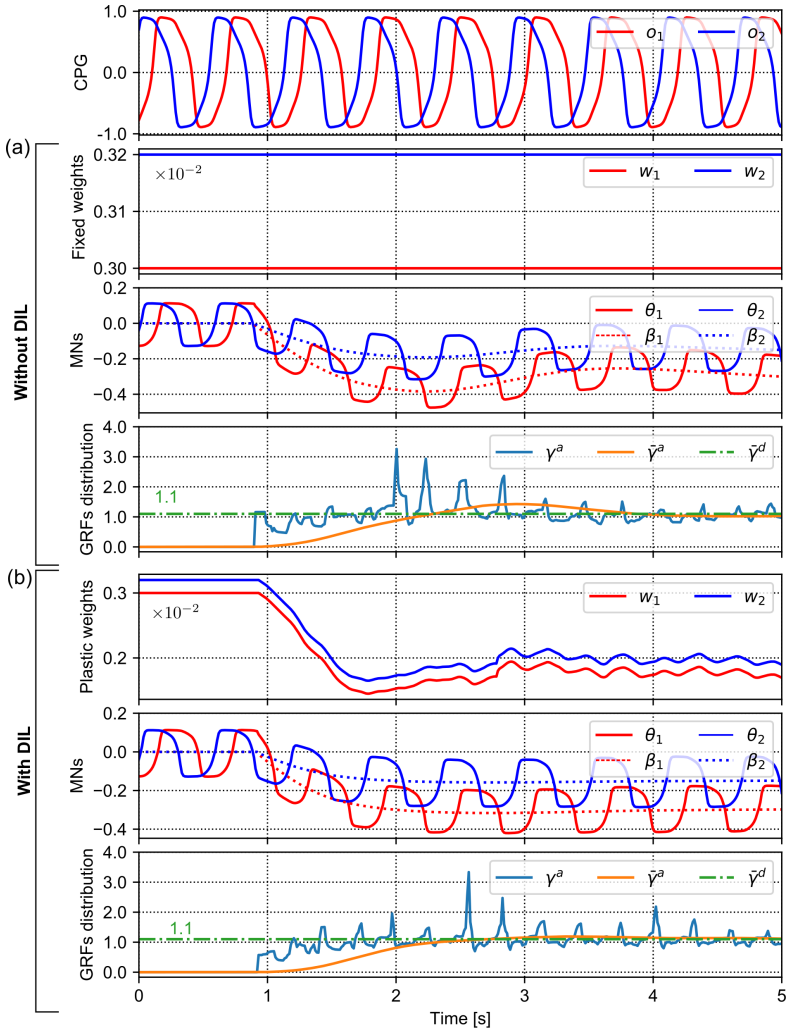

Figure 6: Outputs of the modules ($o_{1,2}$ of a CPG, $w_{1,2}$ adjusted by the DIL, $\beta_{1,2}$ derived from the DFFB reflex, $\theta_{1,2}$ of two MN neurons of a leg, and $\bar{\gamma}$ of the sensory preprocessing unit) in the adaptive quadruped motor control. (a) The DFFB reflex without the DIL. (b) The DFFB reflex with the DIL. Based on the only DFFB reflex, the offsets of MNs' outputs are shifted and the actual $\bar{\gamma}^a$ is gradually converged to the desired value (i.e., $\bar{\gamma}^d \approx 1.1$) after around 4 seconds. $\bar{\gamma}^a$ is also overshoot. In contrast, under the DFFB reflex with the DIL, the plastic weights (w_1 and w_2) are online adjusted to appropriately set the gains of the reflex. This results in a fast convergence of $\bar{\gamma}^a$ within 2 seconds and without overshoot. Note that γ^a represents the actual raw GRFs distribution.

contributes to the adaptation of the joint offsets, are plastic and adjusted online by the DIL. The sensory stimulation changes acquired by N1 serve as an input to the DIL. Specifically, the DIL has two parallel learners with different learning scales [20]. The fast learner has a higher learning rate but a lower retention rate, the slow learner has a lower learning rate but a higher retention rate. The DIL can be described as follows:

$$\begin{aligned} x_f(n) &= A_f \cdot x(n-1) + B_f \cdot e(n) + C_f \cdot \int e(n), \\ x_s(n) &= A_s \cdot x(n-1) + B_s \cdot e(n) + C_s \cdot \int e(n), \\ x(n) &= x_f(n) + x_s(n), \end{aligned} \tag{13}$$

where $x_f(n)$ and $x_s(n)$ are the states of the fast and slow learners, respectively. $A_{f,s}$ are the retention rates. $B_{f,s}$ and $C_{f,s}$ are the learning rates. $e(n)$ is the difference between the absolute values of current and previous N1 outputs of the DFFB reflex network. The DIL does not require precise adjustment of its parameters to fit specific situations. Its further advantages can be seen in [20]. The sum of the fast and slow learner' states ($x(n)$) is set to be the modulation of the synaptic strengths of the network, as shown below:

$$\Delta w_i(n) = x(n), i = 1, 2, \tag{14}$$

where the initial value of the weights ($w_1(0)$ and $w_2(0)$, Fig. 5) are empirically set to 0.003 and 0.0032, respectively.

This synaptic plasticity enables the reflex network with fast online adaptation because the DIL can online adjust the reflex gains (i.e., determined by w_1 and w_2) depending on the sensory stimulation changes (see Fig. 6 (b)). For instance, when the input changes largely (small) the gains increase (decrease) for realizing adaptive synaptic weights (w_1 and w_2). This results in joint offset adaptation.

3. Experiments and Results

In this study, we perform three main experiments on a small-sized quadruped robot (called Lilibot [27]), in simulation (Fig. 7), to evaluate the performance of the DFRL for adaptive quadruped motor control. The experiments consists of: I) trotting on level ground, II) trotting on various slopes, and III) trotting on a complex terrain with multiple slopes (see Fig. 8). The traditional vestibular reflex is also implemented by replacing the DFRL for a comparison. The vestibular reflex utilizes the level body posture strategy by which the robot body is sustained parallel to the horizontal (known as telescoping strut) [17, 42]. It is different from the lever mechanics strategy that utilized by the DFFB reflex in the DFRL. The two strategies can be seen in Figs. A.3 (b) and (c) in Appendix. The scheme of the vestibular reflex is outlined in Fig. A.4 in Appendix. In addition to the comparative experiments on Lilibot, the DFRL is also implemented on a larger quadruped robot (called Laikago, Fig. 7) to demonstrate the DFRL generalization on different platforms.

3.1. Experimental setup

Fig. 7 shows the experimental platforms, Lilibot and Laikago. They are two quadruped robots with different sizes. Their specifications can be seen in Table A.1 in Appendix. The experiments on the robots were performed on three types of terrains, as shown in Figs. 8 (a), (b), and (c). The robots and terrains were built in simulation using CoppeliaSim[4] with Vortex[5]. They, serving as a robot operate system (ROS) node, communicate with the adaptive quadruped motor control through certain ROS topics. The simulation platform with Lilibot and Laikago can be seen in `https://gitlab.com/neutron-nuaa/lilibot`. The control parameters of the DIL used in the following experiments are listed in Table 2.

[4]https://www.coppeliarobotics.com/

[5]A high realistic and precise physical engine: https://www.cm-labs.com/vortex-studio/

To quantitatively evaluate locomotion performance, three global performance metrics (for a whole locomotion process) are induced to measure the stability, coordination, and displacement of robot locomotion based on the adaptive quadruped motor control with the DFRL or vestibular reflex. The definitions of the metrics can be seen in Appendix.

Table 2: The DIL control parameters.

Symbols	Values	Symbols	Values
A_f	0.01	A_s	0.1
B_f	0.05	B_s	0.01
C_f	0.001	C_s	0.0001

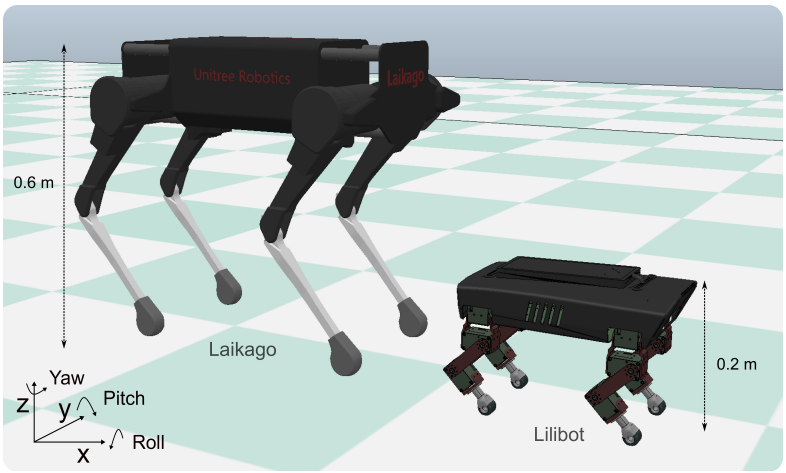

Figure 7: Experimental platforms: Laikago and Lilibot.

3.2. Experiment I: trotting on level ground

The CPG/joint offsets significantly influence the robot's posture in relation to trotting stability, coordination, and displacement. The traditional CPGs-based control of legged locomotion normally requires an additional consideration to robustly predefine the offsets. Here, we perform an experiment to verify

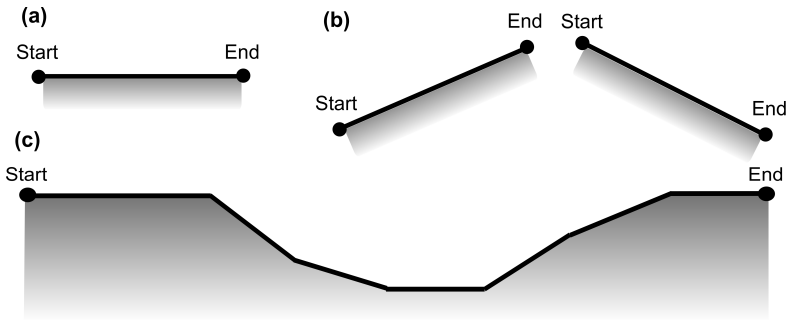

Figure 8: Terrain types used in the three main experiments. (a) Level terrain for experiment I. (b) Uphill and downhill terrains for experiment II. (c) Complex terrain with multiple slopes for experiment III.

whether the proposed DFRL allows the CPGs-based control (Fig. 3) to produce feasible commands with self-adaptive offsets ($\beta_{1,2}$) to maintain stable locomotion. In addition, the vestibular reflex was also tested for comparison.

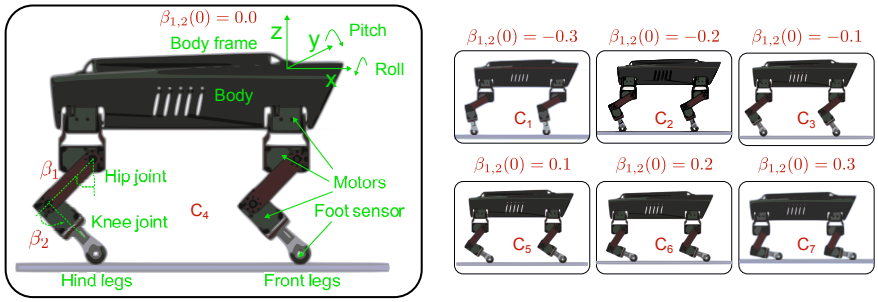

Figure 9: Lilibot configuration and its initialization of postures with corresponding joint offsets ($\beta_{1,2}$) in seven conditions (C_1, C_2, C_3, C_4, C_5, C_6, and C_7).

More specifically, the adaptive quadruped motor control with the DFRL or vestibular reflex was used to drive Lilibot when trotting on level ground with seven different initial offsets (see Fig. 9). The corresponding initial offsets of Lilibot's hip and knee joints in the seven conditions (C_1, C_2, C_3, C_4, C_5, C_6, and C_7) were set to -0.3, -0.2, -0.1, 0.0, 0.1, 0.2, and 0.3, respectively. The test in each condition was preformed five times. At the beginning of every trial, the robot was held in the air to initialize with identical control parameters. After placing the robot on the ground, the DFRL or vestibular reflex was activated.

A video clip of the experiment can be viewed at `http://www.manoonpong.com/DFFB/video1.mp4`.

In this setup, the joint initial offsets in the C_7 condition show the largest deviation from the normal condition (i.e., C_4). Thus, we show the real-time data of a trial in the C_7 extreme condition as an example. The experimental results can be seen in Figs. 10 and 11. In the experiment involving the DFRL, Lilibot quickly formed a regular trot gait and stably moved forward after interacting with the ground (i.e., within five seconds, Fig. 10). In addition, the robot body attitude oscillation decreased significantly. On the other hand, a stable gait could not be formed in the experiment involving the vestibular reflex, where the robot's hind legs always stalled on the ground (see Fig. 11). This results in the higher body attitude oscillation and less forward displacement.

The convergence progress of tests in all conditions, based on the DFRL, can be seen in Fig. 12. One can find that the plastic weights ($w_{1,2}$) of the DFRL are adaptable which affect the changes of the joint offsets ($\beta_{1,2}$). The joint offsets are online adjusted by the DFFB reflex of the DFRL (see Eq. (12)). As a result, the joint offsets of an example leg (i.e., right front leg) quickly converge to particular values in all conditions at different initializations. With the joint offsets being stable, the plastic weights converge into certain values leading to DFFB reflex gains. In addition, the smoothed GRFs distribution parameter ($\bar{\gamma}$) also converges into a constant value of approximately 1.1. After the offsets became stable, so did the robot's posture (i.e., the roll and pitch angles became smaller). However, the results of the experiment using the vestibular reflex (see Fig. 13) did not show any convergence. The joint offsets had almost no adjustment. The GRFs distribution values ($\bar{\gamma}$) spread between 0.0 and 2.0. The robot's posture showed high oscillation in all conditions.

The locomotion performances (*stability*, *coordination*, and *displacement*) can be seen in Figs. 14, 15, and 16. They demonstrate that the adaptive quadruped motor control with the DFRL drives Lilibot to perform higher stability, coordination and longer displacement than the vestibular reflex in almost every tests for all conditions. Specifically, the vestibular reflex driving Lilibot

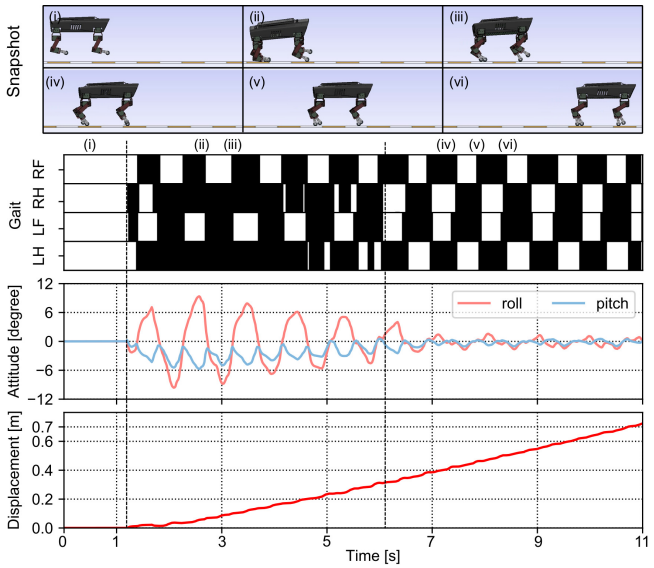

Figure 10: Real-time data of a trial in C_7 condition based on the DFRL. A stable trot gait with less body oscillation emerged after around five seconds. The black area in the gait diagram indicates the stance phase while the white area indicates the swing phase of each leg (RF: right front leg, RH: right hind, LF: left front, LH: left hind).

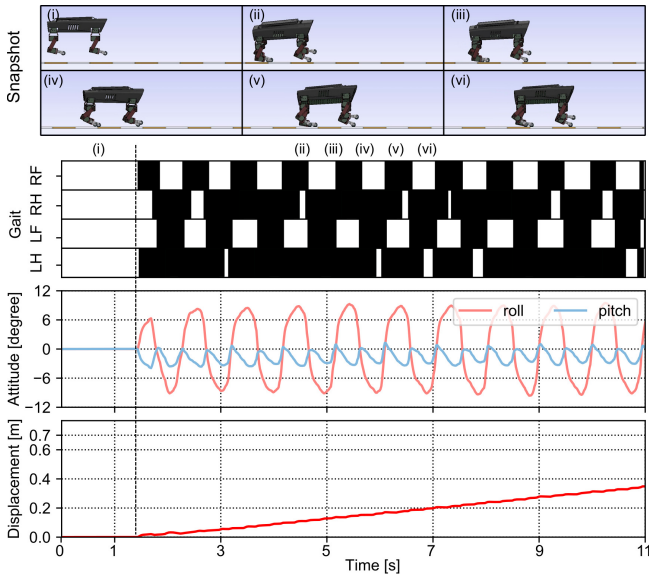

Figure 11: Real-time data of a trial in C_7 condition based on the vestibular reflex. This trial showed no convergence and stable trotting. The black area in the gait diagram indicates the stance phase while the white area indicates the swing phase of each legs (RF: right front leg, RH: right hind, LF: left front, LH: left hind).

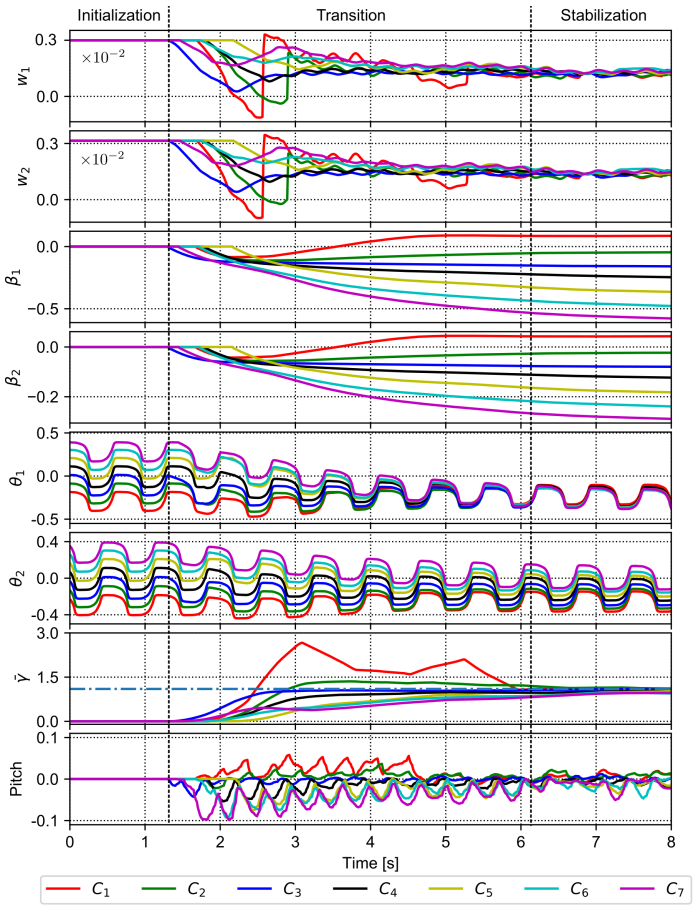

Figure 12: Real-time data for all conditions in experiment I using the DFRL. The progress is divided into three stages including initialization, transition, and stabilization. w_1 and w_2 are the plastic weights of the DFFB reflex network. They are online adjusted by the DIL (see Eqs. (13) and (14)). β_1 and β_2 are the hip and knee joint command offsets of a leg (i.e., the right front leg). They are automatically adjusted by the DFFB reflex (see Eq. (12)). The hip and knee joint commands for the leg are θ_1 and θ_2, respectively. Their offsets converged to constant values within around five seconds. $\bar{\gamma}$ converged to around 1.1. The pitch angle of the robot body, in relation to body stability, obviously became smaller following the offset convergence.

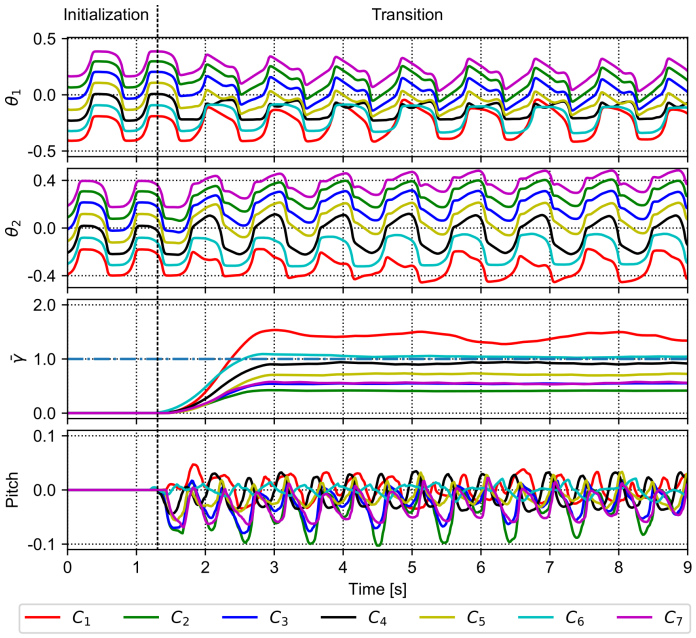

Figure 13: Real-time data of all conditions in the experiment I using the vestibular reflex. This is for comparison with the DFRL (Fig. 12). In this experiment, no convergence was achieved in any conditions.

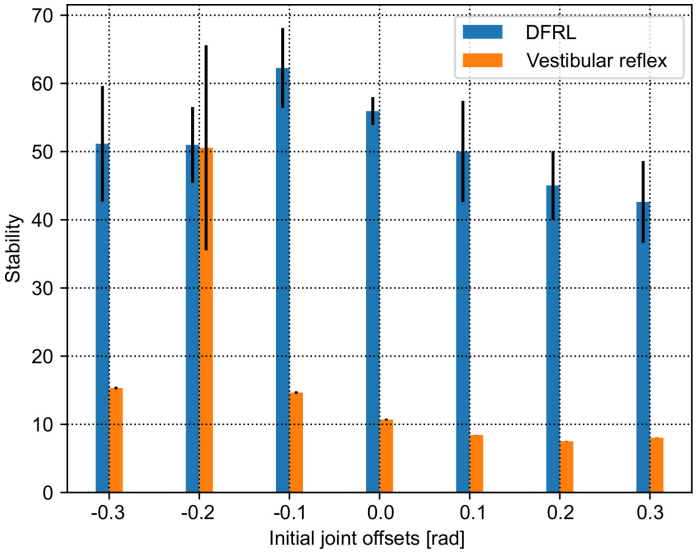

Figure 14: Stability in experiment I. It demonstrates the comparative result of the DFRL and vestibular reflex. The DFRL outperforms the vestibular reflex. The best performance of the vestibular reflex occurred in the C_2 condition where the joint offsets were initially set to -0.2. (see Fig. 9)

only shows enough stability in the C_2 condition (-0.2) (see Fig. 14). The plot in Fig. 15 shows the coordination performance. The DFRL outperforms the vestibular reflex in all conditions. The plot in Fig. 16 shows the displacement. The robot with the DFRL traverses almost the same displacement in all conditions. However, the most suitable joint offsets for the vestibular reflex only occur in the C_2 condition. Since the joint offsets of the C_2 condition are the best setup for the vestibular reflex, we used these as initial offsets for the following slope experiments. In summary, the results of experiment I demonstrate that the DFRL enables the robot to quickly learn and adapt its joint offsets in any initial conditions for stable trotting on level ground.

3.3. Experiment II: trotting on various slopes

In this experiment, we comparatively assess the effectiveness of the DFRL and vestibular reflex when they are used to stabilize quadruped robots (i.e., Lilibot) trotting on slopes. A series of slope terrains ($-35°$, $-30°$, $-20°$, $-10°$, $0°$, $10°$, $20°$, $30°$, and $35°$) were used for testing. Note that the negative and positive angles indicate declined and inclined slopes, respectively. Each test using the DFRL or vestibular reflex on a terrain was performed repeatedly five times. At the beginning of all trails, the robot was initialized with the same state by holding it in the air, after that it was dropped on the ground to trot forward. Afterwards, it approached a slope with its front legs. The change of the terrains (from level ground to a slope) presented a challenge for the robot since it needed to adjust its posture to adapt to the transition and a new terrain using its reflex mechanism.

The real-time data on the experiment involving the most challenging slopes ($35°$ and $-35°$) are depicted first, followed by the experiment statistic for all slopes. A video clip of the experiment can be viewed at `http://www.manoonpong.com/DFFB/video2.mp4`.

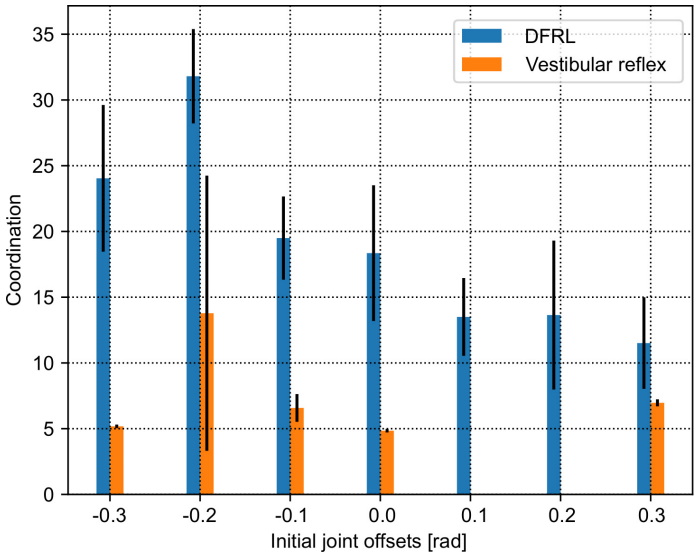

Figure 15: Coordination of experiment I. It demonstrates the comparative result of the DFRL and vestibular reflex. The DFRL obviously contributes to better coordination in all conditions. The best coordination of the vestibular reflex occurred when the joint offsets were initially set to -0.2 (C_2, see Fig. 9). For the vestibular reflex in the two conditions (C_5 and C_6) where joint offsets were set to 0.1 and 0.2, the coordination was zero due to certain legs always stalled on the ground during the whole locomotion period.

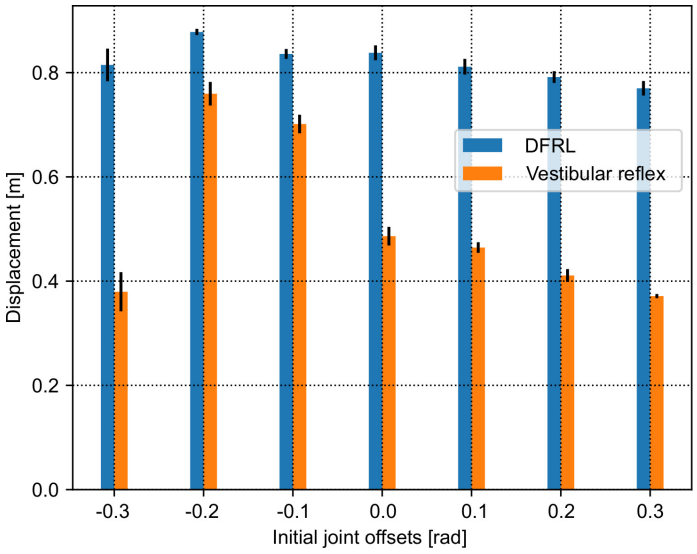

Figure 16: Displacement of experiment I. Lilibot driven by the DFRL walked longer with displacement than the robot driven by the vestibular reflex in all conditions. Under the vestibular reflex, the robot performed best when its joint offsets were initially set to around -0.2 (C_2).

3.3.1. Feasible maximum slope

Under the DFRL, Lilibot can trot on inclined and declined slope terrains of $\pm 35^\circ$. For comparison, the real-time data on the experiment controlled by the vestibular reflex id also depicted. The adjustment effects of the DFRL and vestibular reflex can be seen in Figs. 17 and 18.

The joint commands of a leg (i.e., the right front (RF)), $\bar{\gamma}$, body posture angles (i.e., pitch and roll), displacement, and gait diagrams are plotted. The locomotion can be divided into three stages: locomotion on level ground (S1 stage), transition from level ground to a slope (S2 stage), and locomotion on the slope (S3 stage).

The experimental results on the 35° slope can be seen in Fig. 17. Under the DFRL (Fig. 17 (a)), the joint commands and $\bar{\gamma}$ quickly converged during the S1 and S3 stages after the robot was placed on the ground or crossed the terrain transition. $\bar{\gamma}$ eventually was around 1.1. Besides, the robot pitch angle approximated to the slope inclination (35°) in the S3 stage. This means the robot successfully trotted on the 35° slope. The robot roll angle showed little oscillation during the convergence period (in the S1 and S3 stages). The gradient (velocity) of the displacement curve became lower during the uphill locomotion in the S3 stage. This is because the amplitudes of the joint movement commands became smaller, and thus caused a shorter step length. The final plot, in the gait diagrams, also shows more regularity during the stabilized stages (S1 and S3), which means the robot had a stable trot gait. The gait diagram also indicates that the hind legs (RH and LH) had larger duty factors than the front legs (RF and LF) in S2. This reflects that the loads was mainly on the hind legs. As for the vestibular reflex (Fig. 17 (b)), although the joint commands also showed changes when the robot touched the inclined slope, the robot got stuck at the bottom of the slope during the entire test period. Therefore, $\bar{\gamma}$ did not converge to the expected value (i.e., 1.1) and the pitch angle did not approximate to the slope angle.

The experimental results on the -35° slope can be seen in Fig. 18. Under

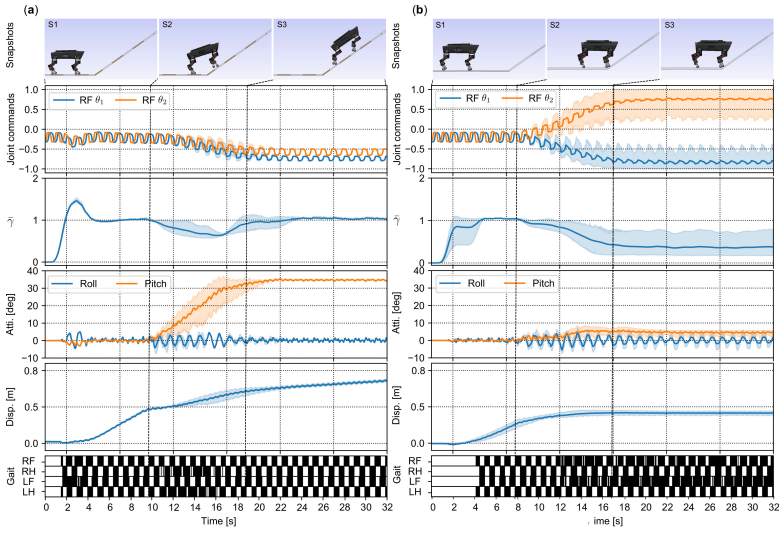

Figure 17: Real-time data of Lilibot when trotting from the level ground to the 35° inclined slope. (a) The robot driven by the DFRL. (b) The robot driven by the vestibular reflex. The black and white areas in the gait diagram indicate stance and swing phases, respectively. RF, RH, LF, and LH represent the right front, right hind, left front, and left hind legs, respectively.

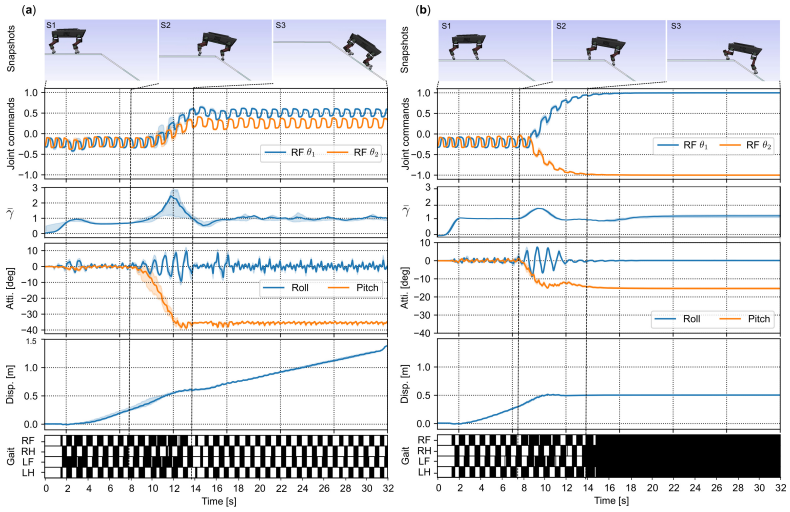

Figure 18: Real-time data of Lilibot when trotting from the level ground to the 35° declined slope. (a) The robot driven by the DFRL. (b) The robot driven by the vestibular reflex. The black and white areas in the gait diagram indicate stance and swing phases, respectively. RF, RH, LF, and LH represent the right front, right hind, left front, and left hind legs, respectively.

the DFRL (Fig. 18 (a)), the joint commands and $\bar{\gamma}$ also quickly converged in the S1 and S3 stages. $\bar{\gamma}$ eventually was also around 1.1. The pitch angle and displacement curves indicate that the robot successfully trotted forward on the $-35°$ slope. The gait diagram also shows a regular pattern during the S1 and S3 stages. Conversely, under the vestibular reflex, the results show that the robot failed to walk on the $-35°$ slope (Fig. 18 (b)). This is because that the joint commands reached their limits (i.e., ± 1.0 rad) due to the vestibular reflex, thus the robot stopped.

Consequently, the adaptive quadruped motor control with the DFRL enables Lilibot to perform stable trotting on steep slopes ($35°$ and $-35°$), while the adaptive quadruped motor control with the vestibular reflex is unable to do so.

3.3.2. Statistical analysis

Lilibot was driven by either the adaptive quadruped motor control with the DFRL or vestibular reflex to trot on every slope terrain five times. The number of times the control successfully implemented on different slope terrains are shown in Fig. 19. It shows that Lilibot, under the DFRL, can trot on all the listed slope terrains, while under the vestibular reflex could only trot on $-10°$, $0°$, $10°$, and $20°$ slopes. The statistical locomotion performance of the two reflexes can be seen in Figs. 20, 21, and 22.

As shown in Fig. 20, the DFRL exhibited greater stability than the vestibular reflex. Moreover, the steeper the slope, the greater the stability of the DFRL. This is because the step length became shorter on slopes with higher inclination (see joint commands in Fig. 17 (a)). Under the vestibular reflex, the robot locomotion showed the greatest stability on the flat ($0°$). This is because the initial offsets (i.e., -0.2) of the joint commands were the most suitable for level ground (see Figs. 14, 15, 16).

As shown in Fig. 21, the DFRL has more coordination than the vestibular reflex. Furthermore, the DFRL and the vestibular reflex exhibited the best coordination on level ground. This is because the initial command offsets were most suited to level ground locomotion for which the GRFs distribution ($\bar{\gamma}$) was

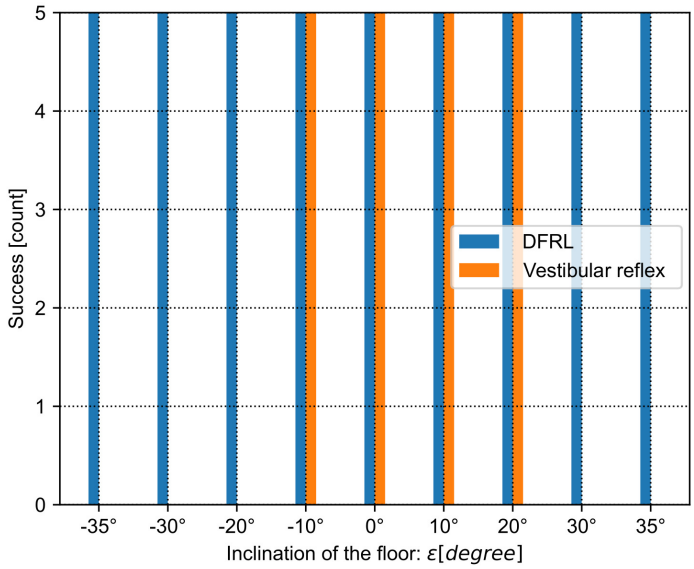

Figure 19: Number of times Lilibot successfully exhibited locomotion on various slopes. The comparison between the adaptive quadruped motor control with the DFRL and the vestibular reflex.

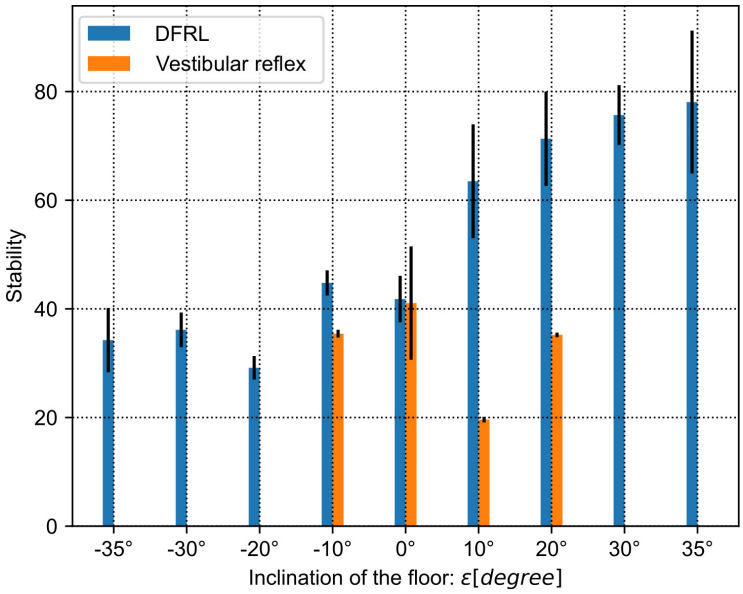

Figure 20: Stability of Lilibot locomotion on various slopes. The adaptive quadruped motor control with the DFRL and vestibular reflex driving Lilibot are compared.

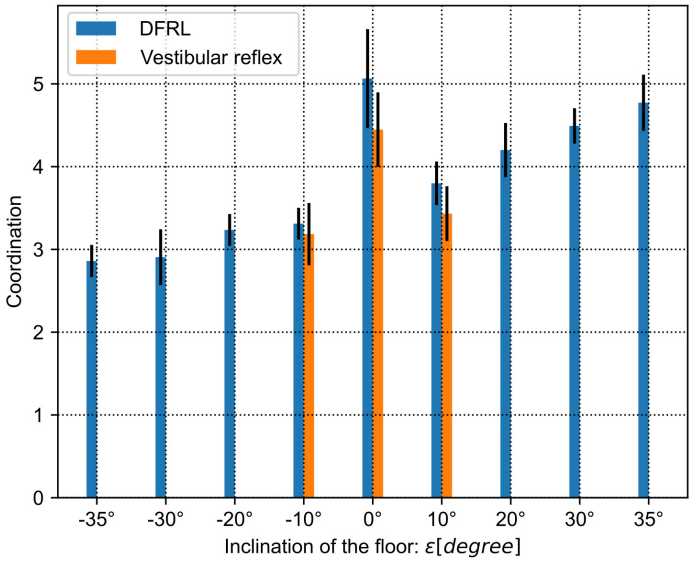

Figure 21: Coordination of Lilibot locomotion on various slopes. The adaptive quadruped motor control with the DFRL and vestibular reflex driving Lilibot are compared.

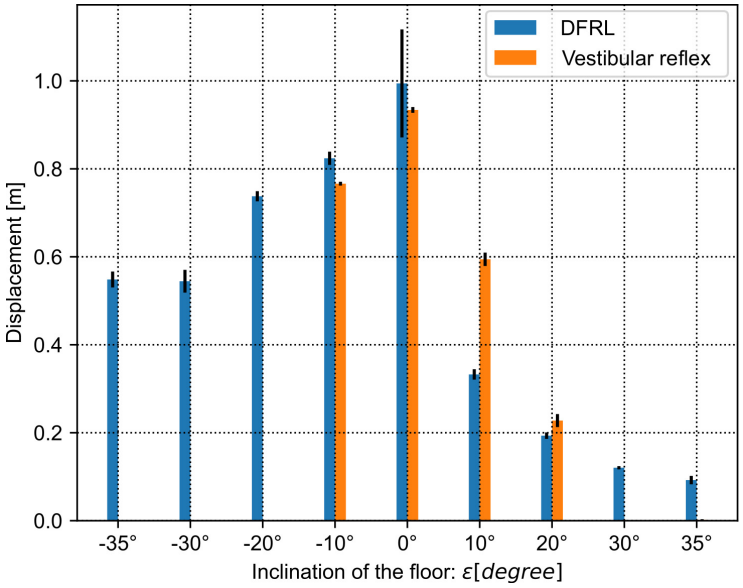

Figure 22: Displacement of Lilibot locomotion on various slopes. The adaptive quadruped motor control with the DFRL and vestibular reflex driving Lilibot are compared.

already in the desired condition. Besides, the coordination of the DFRL shows a slight uptrend with the inclinations. This is because the robot had short step length on higher inclination (see joint commands in Fig. 17 (a)), which benefits the coordination to some extent. In addition, the coordination of the vestibular reflex at 20° was zero. This is because the hind legs always stayed on the ground even when the robot trotted on the uphill. In other words, the hind legs had no swing phase.

Fig. 22 shows that the closer the slope is to level ground, the longer the displacement of the DFRL or vestibular reflex. This results from that the robot has the greatest coordination, larger stability, a longer step length on level ground. The displacement on downhill is longer than on uphill, this success can be attributed to the gravity pushing the robot forward on the downhill while pulling the robot on the uphill. It should be noted that the robot under the vestibular reflex on 10° and 20° slopes exhibited a longer displacement than under the DFRL. This is because, on the one hand, the DFRL shortened the step length during the uphill locomotion and the stable trot gaits on uphill generated higher foot touch impulse force causing a short deceleration process. On the other hand, the robot under the vestibular reflex showed an irregular trot gait or walking gait which sustained the robot with a constant forward movement.

3.4. Experiment III: trotting on a complex terrain with multiple slopes

In this experiment, Lilibot, under the DFRL, was conducted to trot on a complex terrain with multiple connected slopes (Fig. 8). This scenario simulates the irregularity of the natural ground. From this test, the smoothness of the diverse-slope transition could be assessed. Moreover, the locomotion characteristics on different slopes could be compared continuously. A video clip of this experiment can be viewed at `http://www.manoonpong.com/DFFB/video3.mp4`.

The experimental results can be seen in Fig. 23. The joint commands of a leg (i.e., the right front leg) adapt to changes of the slope inclinations. The curve of $\bar{\gamma}$ indicates the GRFs distribution. It shows a significant change during

the terrain transition, while quickly reaching a convergence of around 1.1 in non-transition. The pitch angle can directly reflect the slopes on which the robot was trotting. According to the displacement plot, the locomotion on declined slopes is faster in comparison to that exhibited on the inclined slopes. It is obvious from the gait diagram that the robot exhibited greater regularity in its trot gait when walking on the inclined slopes. This means that the robot acquired better GRFs distribution in comparison to that exhibited on the declined slope. To sum up, the adaptive quadruped motor control with the DFRL can enable the quadruped robot to trot on complex slope terrain.

3.5. Generalization test on Laikago

The adaptive quadruped motor control with the DFRL was also implemented on Laikago in simulation. The control developed for Lilibot without any modifications was directly transferred to Laikago. The experimental results show that the proposed control can not only make Laikago self-stabilize its body posture regardless of its initial posture on level ground, but also trot on different slopes with an inclination up to 50° inclined (see Fig. 24) as well as -45° declined. A video clip of the experiment can be viewed at `http://www.manoonpong.com/DFFB/video4.mp4`.

4. Discussion

In this paper, we propose adaptive quadruped motor control based on the integration of CPGs, sensory feedback, reflex, and online (motor) learning. The control is realized using neural CPGs-based control and the DFRL (Fig. 2). The DFRL consists of the DFFB reflex and the DIL. The DFFB reflex, organized by a neural network with synaptic plasticity, can adjust the CPG/joint offsets depending on the GRFs distribution (Fig. 5). The associated DIL is used to online modulate the plastic synapses (w_1 and w_2, Eq. (14)) of the DFFB reflex network. This improves the DFFB reflex with faster adaptation (Fig. 6). The experimental results show that the DFRL can efficiently generate the adaptive

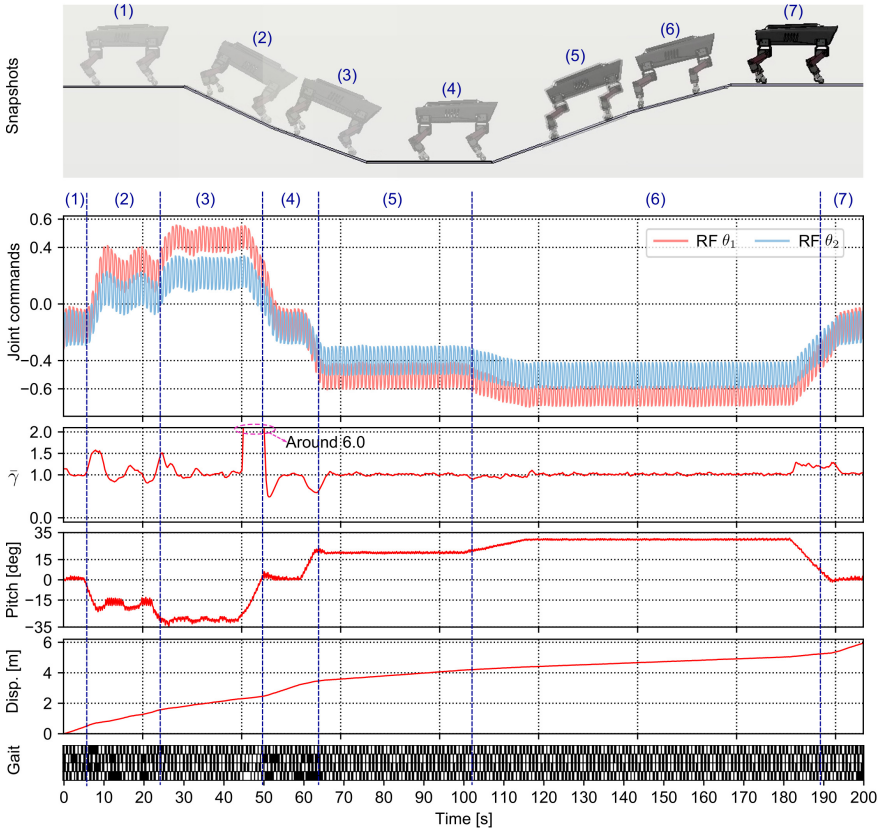

Figure 23: Real-time data of Lilibot trotting on a complex slope terrain. The top graph refers to the motion scene of the robot. It also indicates the complex slope terrain composed of two flat floors as well as several declined and inclined slopes. The plots represent the joint commands of a leg (i.e., RF), $\bar{\gamma}$, pitch angle of the robot body, displacement of robot locomotion, and gait diagram, respectively. The bars from the top to the bottom in the gait diagram indicate the right front, right hind, left front, and left hind legs, respectively. The black area represents the stance phase while the white area represents the swing phase.

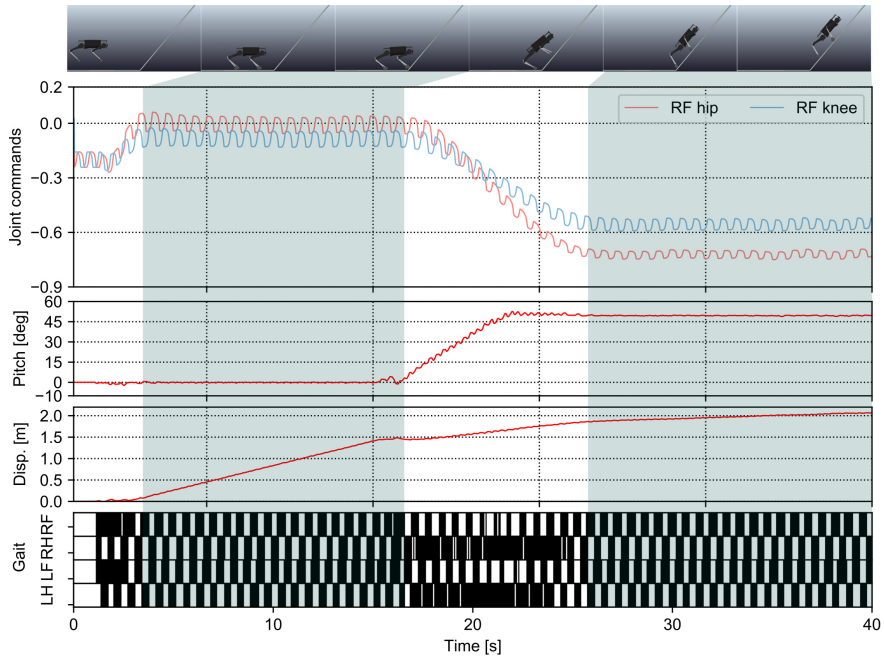

Figure 24: Laikago trots on a 50° inclined slope. The black areas in the gait diagram represent the stance phase while the white areas represent the swing phase. RF, RH, LF, and LH represent the right front, right hind, left front, and left hind legs, respectively.

CPG/joint offsets, and thus enable quadruped robots to quickly adapt their posture against different initial offsets on level ground (experiment I), stably trot on steep slopes (experiment II), and properly handle a complex terrain with multiple slopes (experiment III). Moreover, the adaptive quadruped motor control developed for Lilibot can be directly implemented on Laikago (Fig. 24). This demonstrates the generalization of the proposed control on quadruped robots of different sizes and weights without the need for robot models. In summary, the work concerns two subtopics: 1) how to realize CPG/joint offset adaptation using biological mechanisms for obtaining stable trotting of quadruped robots and 2) the application of the CPG/joint offset adaptation on diverse slope terrains. The remaining issues concerning the two subtopics are discussed in the following paragraphs.

A genuine bio-inspired control is model-free in contrast to the control using engineering control techniques (e.g., whole body control [7], inverse dynamic model-based control [5], optimization-based control [8], and MPC [9]) and has faster convergence compared to RL approaches [31, 32, 33, 34]. Although many quadruped robots with bio-inspired control have not demonstrated such high performance as that reported in the well-known works (e.g., BigDog [43], MIT Cheetah [4], and ANYmal [32]), bio-inspired control has promising potential for generating versatile animal-like movement along with the progress of biological investigation [1, 11, 44]. Therefore, it is reasonable to expect that a generic, efficient, and adaptive control framework for quadruped robots can be realized through the development route of biologically inspirations.

Towards this goal, the DFRL has been developed. Its strategy is inspired by a biomechanical finding (i.e., lever mechanic [29]) for sustaining body posture stabilization on various terrains (Fig. 8). It is constructed using a neural network in which the key synapses (w_1 and w_2) can be adjusted online by the DIL (Fig. 5). The DIL has two parallel learners with different rates (Eq. (13)). This DIL feature provides the DFFB plastic synapses with two different time-scale adaptations. Moreover, this also results in the DFRL with two different level adaptations: internal synapse adaptation (Eq. (14)) and external offset adap-

tation (Eq. (12)). For instance, when robots traverse on different slopes, their GRFs distribution changes. On the one hand, this activates the DFFB reflex to adjust the robot posture. On the other hand, the DIL is also functioned to increase the network synaptic strength, thereby resulting in high reflex gains. After the changes of the GRFs distribution become small, the DIL decreases the synaptic strength to acquire lower reflex gains for fine modulation (Fig. 12). The synaptic plasticity is quite useful for overcoming the long delay induced by the sensory acquisition and preprocessing of the DFFB reflex. Otherwise, the delay would cause the reflex modulation procedure to become very slow with low weights (i.e., w_1 and w_2) or unstable with high ones (Fig. 6). The functionality of the DIL can be analogous to serotonin (5-HT) neurons in a biological system, which releases 5-HT in the spinal cord to modulate synaptic strengths of interneurons in a locomotive neural network [45, 46, 47, 48, 49].

In addition to the flexibility and adaptations due to the DIL, the DFRL is also intrinsically modular and independent of specific CPG model formats as well as the size and weight of robots. Thus, it can easily be integrated into diverse CPGs-based control, and also facilitates generic adaptive quadruped motor control with CPG offset adaptation for different quadruped robots. Furthermore, the DFRL can also be conveniently integrated with other CPG adaptation techniques, such as phase adaptation [19] and frequency adaptation [20], hence resulting in CPGs-based control with phase, frequency, and offset adaptations. This will substantially expand the applicability of bio-inspired CPG-based control. In a word, this study helpfully paves the way for developing more advanced bio-inspired control with more adaptation and generalization, and also, on the other hand, shed light on the neurological locomotion control to some extent. It also demonstrates how to efficiently manipulate sensory information through a neural system with plasticity for adaptive motor control in robotic systems.

However, the realization techniques for the DFRL, in this paper, still have some limitations. Firstly, it is a compromising way to use the averaged/smoothed GRFs distribution $\bar{\gamma}$ as sensory feedback for the DFFB reflex (see Eq. (11)). Ideally, the GRFs distribution should be measured while the stance/swing phase

switching on which the GRFs distribution ($\gamma(n_0)$) of a stable trot gait is determined 1.0 (Fig. 4 (b)). The use of the averaged GRFs distributions causes three drawbacks: 1) inducing an additional empirical parameter (i.e., sample size N in Eq. (11)); 2) inducing a larger delay effect in the sensory preprocessing module due to the moving-average filter; 3) decreasing the robustness since the desired $\bar{\gamma}$ (i.e., 1.1) related to a specific step length and period (see Fig. 4 (b)). Therefore, an improved sensory preprocessing module for acquiring the instant GRFs distribution of a switching moment should be developed in future work.

In addition, although the CPG offset adaptation shows fast convergence, i.e., within two seconds (see Fig. 6), it cannot handle the need for a sudden emergency response, such as avoiding the robots falling down from an unexpected step. Thus, the proposed control needs to be combined with other instant reflexes to deal with such an emergency situation. For instance, a flexion reflex prevents the robot from falling down, sideways stepping reflexes stabilize the rolling motion, and corrective stepping reflexes deal with walking down stepping [50].

Over the past few decades, quadruped locomotion on slopes has been an interesting research topic in both animals and robotics, which represents a fundamental characteristic of quadrupeds toward adaptive locomotion on natural environments [26, 17, 51, 30, 52, 29, 53]. Quadruped locomotion on slopes is generally a more complicated task compared to locomotion on level ground since it involves four extra constraints: 1) postural correction for maintaining balance on slopes [29]; 2) flexible joint motion generation to accommodate the transitions from different terrains (such as from flat surfaces to slopes) [54]; 3) a sufficient motor power supply to overcome the effect of appended loads on uphill [53]; 4) an adequate feet tangential force for avoiding slippage caused by gravitational compensation on the slope [30]. The former two conditions, i.e., balance and transition, relating to body and joint movement can be handled by enhanced locomotion control techniques. The latter two factors, i.e., motor power and friction force, deterministically depend on robot mechanics and material. To

explore the two control issues of slope locomotion, a variety of approaches have been proposed and implemented on quadruped robots.

A vestibular reflex has been proposed to generate adaptive dynamic running on unperceived slopes, where the slopes are regarded as disturbances in many works [23, 24, 25, 26, 17, 27]. Specifically, the vestibular reflex is used to shift the offsets of joint movement commands, originally produced by CPGs, so as to extend or flex the legs, thereby maintaining the robot body parallel to the horizontal (see Fig. A.3 (b)). In addition, a vestibular reflex has also been applied to adjust the frequency and amplitude of the joint movement commands by Zhao et. al. in few works [28]. That demonstrates a quadruped robot AIBO to steadily trot on slight slopes using high step frequency and short step length. Despite the successful implementation of the vestibular reflexes in these cases, they are all limited to low slopes (less than $20°$, see Table 1).

In contrast to the vestibular reflexes, the DFFB reflex can translate the ZMP coordination into a proper position along the slope direction. In this way, the robot body orientation is aligned to the slope when the stability margin is increased (see Fig. A.3 (c)). As a result, the front and hind legs are in a much more natural pose to significantly distance themselves from singular configurations or joint limits. Thus, the robots can adapt to higher slopes. The two distinct strategies, body orientation parallel to the horizontal and parallel to the slope, are known in biomechanics as the telescoping strut and lever mechanics, respectively [29]. Unfortunately, the vestibular reflex cannot inherently carry out the lever mechanics strategy because it requires the body orientation to be parallel to the slope rather than the horizontal. Whereas the DFFB reflex based on the lever mechanics strategy can enable quadruped robots to trot on steep slope terrains (e.g., $35°$ for Lilibot and $-45°$ and $50°$ for Laikago).

To reveal the relationship between the joint offsets and slope inclination on which the quadruped robots can trot, we provide an analysis of the underlying mechanism using a simplified quadruped robot model (see Appendix). The analytical model can not only prove the functionality of the DFFB reflex strategy, but also predict the maximum inclination on which quadruped robots can trot

without considering the friction, joint torque limit, asymmetric structure etc. Moreover, the analytical results match the simulation results.

Furthermore, the MNs in CPGs-based control also have the advantage of stabilizing robot locomotion on slopes. This is because the MNs can scale the joint command amplitudes to kindly shorten the step length and height on slopes when MNs offsets are shifted. For instance, when robots trot on a slope, the MNs offsets will be shifted closely to the saturation zones of the MN transfer function (i.e., sigmoid Eq. (7)) due to the DFFB reflex. As a result, the joint command amplitudes will be decreased, and then the robot step length and height are reduced, which benefits the stabilization of the robots on slopes (see Fig. 17). This fits the biomechanical investigation finding in animals [55].

5. Conclusion

This paper demonstrates that the adaptive quadruped motor control with the DFRL can enable quadruped robots to stably trot on diverse slope terrains. This results from the DFRL automatically realizing adaptive CPG/joint offsets to obtain appropriate robot posture depending on GRFs distribution. Moreover, the adaptability and flexibility of the DFRL are significantly improved by the learning mechanism DIL, which online modulates the property (reflex gains) of the DFFB reflex network of the DFRL. As a result, the DIL make the DFRL has faster adaptation and more generalization on different platforms with different sizes and weights (e.g., Lilibot and Laikago).

Appendix A. Stability analysis of a quadruped robot trotting on slopes using a simplified model

Appendix A.1. Modeling

Intuitively, the stable trotting of a quadruped robot on slope terrains is a complicated task involving many aspects (control, structure, material, power,

and friction etc.) which are required to meet certain specific conditions as described in the discussion section. In this paper, we focus on body posture stability regarding for stable locomotion. Fig. A.1 illustrates a simplified quadruped robot model for analyzing body posture stability conditions when a quadruped robot trots on a slope. In this analytical model, we assume that: 1) the leg mass is negligible and the center of mass (CoM) is located in the center of the body since most of the robot's mass is located in its base; 2) Coriolis and centrifugal forces are negligible (this is reasonable because in our experiments the robot moves slowly); 3) the feet dot not slip on the surface (feet are enacted with enough friction force) and cannot generate moments at the contacts since the feet have nearly point contact area [56]. Based on these assumptions, a equilibrium constraint of the stability conditions, which satisfies both front and hind stance feet lifting as planned, can be described as follows:

$$F_h \cdot x_1 = F_f \cdot x_2 \tag{A.1}$$

From geometric relationship of the model in Fig. A.1, we can get the following equations:

$$\begin{aligned} x_1 &= y_1 - \delta_y, \\ x_2 &= y_2 + \delta_y. \end{aligned} \tag{A.2}$$

By the leg's forward kinematics, the variables in Eq. (A.2) can be expressed as follows:

$$\begin{aligned} \delta_y &= (H/2 + l_0 + h_{hip}) * tan(\eta), \\ y_1 &= L/2 + l_1 * sin(\theta_1^a) - l_2 * sin(\theta_2^a - \theta_1^a), \\ y_2 &= L/2 - l_1 * sin(\theta_1^a) + l_2 * sin(\theta_2^a - \theta_1^a), \end{aligned} \tag{A.3}$$

where L and H are the length and height of the robot body. $l_{0,1,2}$ are the length of the leg links, h_{hip} is the height of the hip to the substrate. $\theta_{1,2}^a$ are the anterior extreme positions of the hip and knee joints, which can be determined by the joint command offsets.

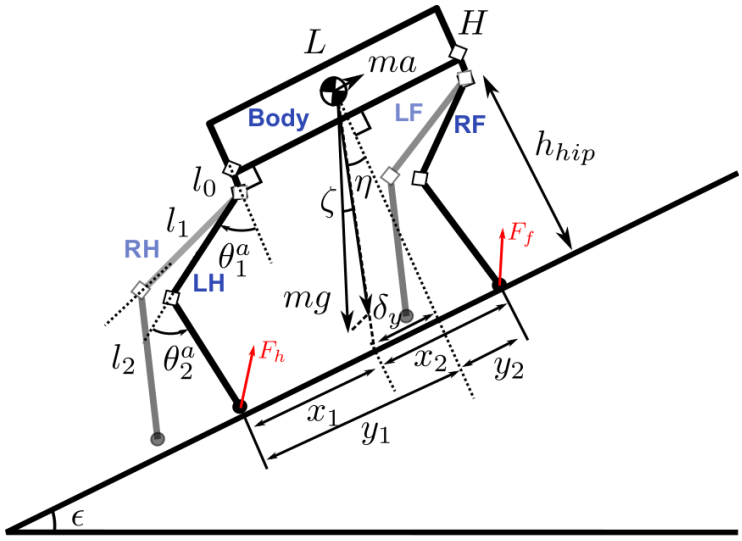

Figure A.1: Simplified model of a quadruped robot trotting on a slope in the sagittal plane. The robot is modeled as a rigid body connected to four identical legs, each of which consists of three connected links without mass, l_0, l_1, and l_2. The mass of the body m is located at its base, and the dimensions of the body are referred to as $L \cdot H$. ma and mg represent the inertial force and gravity being acted on the body, respectively. $\theta^a_{1,2}$ are the anterior extreme position of hip and knee joints, respectively. F_f and F_h represent the front and hind GRFs, respectively. ϵ represents the slope inclination.

From the geometric restrictions, we can get h_{hip} and η in Eq. (A.3) as bellows:

$$\begin{aligned} h_{hip} &= l_1 * cos(\theta_1^a) + l_2 * cos(\theta_2^a - \theta_1^a), \\ \eta &= \epsilon - \zeta, \end{aligned} \tag{A.4}$$

where ϵ indicates the slope inclination.

By combining Eqs. (A.1), (A.2), (A.3), and (A.4), we get the relationship between the joint anterior extreme positions ($\theta_{1,2}^a$) and the slope inclination (ϵ), on which the robot can steadily trot without considering the other conditions (i.e., joint torque limit, feet friction force, uneven surface, etc.), as below:

$$\begin{aligned} \epsilon = arctan(\frac{l_1 * sin(\theta_1^a) - l_2 * sin(\theta_2^a - \theta_1^a)}{H/2 + l_0 + l_1 * cos(\theta_1^a) + l_2 * cos(\theta_2^a - \theta_1^a)}) \\ +\zeta. \end{aligned} \tag{A.5}$$

Assuming $\Delta\theta_{1,2}$ represent the joint movement ranges of the hip and knee joints, then we can get the joint command offsets:

$$\beta_{1,2} = \theta_{1,2}^a - \Delta\theta_{1,2}/2. \tag{A.6}$$

Based on Eqs. (A.5) and (A.6), the relevance of the joint command offsets ($\beta_{1,2}$) and conquerable slopes (ϵ) are expressed. Although this derivation ignores certain realistic restrictions, it not only proves the reason why the proper joint command offsets can stabilize the trotting of quadruped robots on slopes, but also provides a quantitative guideline for modulating the offsets for trotting stabilization, thereby predicting the maximum slope inclination on which a quadruped robot can trot according to its leg and body dimensions, as well as joint movement ranges (l_0, l_1, l_2, H, $\Delta\theta_{1,2}$).

Appendix A.2. Maximum slope inclinations on which Lilibot and Laikago can trot

Based on the foregoing conclusion, we can calculate the maximum inclination of the slope that Lilibot is able to handle. The configuration of Lilibot can be seen in Table A.1. Substituting these parameters in Eq. (A.5), we get a

Table A.1: The main specifications of Lilibot and Laikago.

Parameters[2]	Values	
	Lilibot	Laikago
m	2.5 Kg	25 Kg
H	0.07 m	0.15 m
L	0.32 m	0.55 m
l_0	0.04 m	0.08 m
l_1	0.07 m	0.41 m
l_2	0.086 m	0.45 m
θ_1^a	0° - 80°	0° - 85°
θ_2^a	50° - 110°	50° - 110°
ζ	0°	0°
Total DOFs	12	12
Force sensors	4	4

visualization of conquerable slopes in Fig. A.2. The graph reveals that the maximum slope inclination (ϵ_{max}) on which Lilibot can trot is around 35.6° when $\theta_1^a = 80°$, $\theta_2^a = 50°$, while the minimum (ϵ_{min}) is around $-36.2°$ when $\theta_1^a = 0°$, $\theta_2^a = 110°$. For Laikago, $\epsilon_{max} = 50°$, when $\theta_1^a = 85°$, $\theta_2^a = 50°$, $\epsilon_{min} = -45.8°$ when $\theta_1^a = 0°$, $\theta_2^a = 110°$. Note that these results are based on three assumptions: the feet can obtain sufficient friction force, the joint motor can provide sufficient power, and the inertial force (ma) can be ignored since the locomotion speed is quite slow.

Appendix B. Postural modulation strategies for slope locomotion

A quadruped robot trotting on a slope requires additional body posture modulation to maintain stability. There are two postural modulation strategies:

[2] $\theta_{1,2}^a$ are determined depending on the joint structure configuration. ζ can be approximately set as zero when the robot with a quite low walking speed.

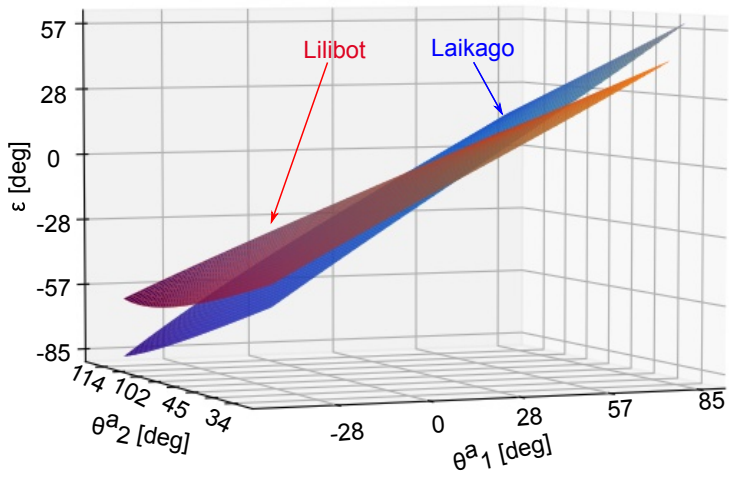

Figure A.2: Visualization of the relationship between the joint anterior extreme positions and conquerable inclined slopes of Lilibot and Laikago.

telescoping strut and level mechanics (see Fig. A.3).

Without a postural modulation strategy (see Fig. A.3 (a)), gravity places a highly load on the hind legs of the robot during uphill locomotion, thus the x_1 is significantly smaller than x_2. This means that γ is smaller than a standard value. Consequently, the hind legs are unable to lift. Conversely, under either of these two strategies, with postural modulation the GRFs distribution or γ would be appropriate for stably lifting the feet. Nevertheless, they are effective in different ways.

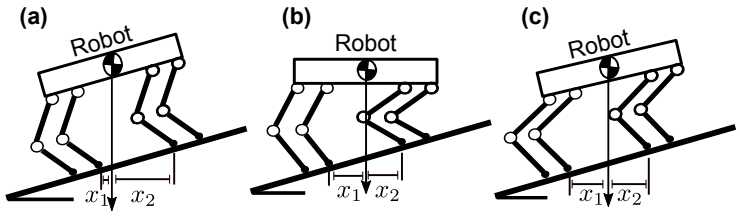

Figure A.3: Strategies of postural modulations for quadruped robots trotting on slopes. (a), (b), and (c) are the strategies: no postural modulation, telescoping strut, and lever mechanics respectively.

Appendix C. Vestibular reflex mechanism

The vestibular reflex mechanism can be seen in Fig. A.4. The reflex utilizes body posture angles (i.e., pitch and roll) as sensory feedback to activate a response. The outputs of the reflex are transferred to the MNs to adjust the CPG/joint offsets. As a result, the joint movements are adjusted to obtain a level body posture.

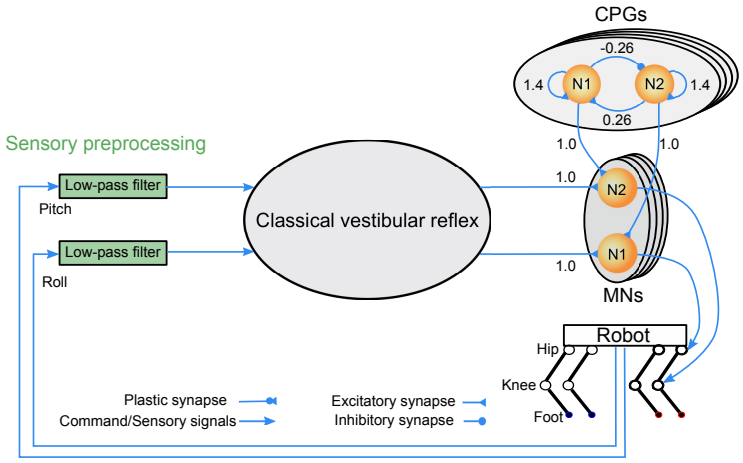

Figure A.4: Diagram of CPGs-based control with the vestibular reflex. The reflex adjusts robot posture on slope using the telescoping strut strategy [27].

Appendix D. Performance metrics

Appendix D.1. Stability

As we know, large amplitude changes in body orientation (i.e., roll and pitch) decrease locomotion stability, i.e, negatively affecting the conservation of momentum and increasing the possibility of the robot falling [57, 58]. The pitch angle is influenced by the slopes on which the robot is trotting. Therefore, only the maximum standard deviation of the body roll angle is used to reflect its stability during a locomotion period. The detailed definition is described as:

$$\bar{roll} = \frac{1}{N}\sum_{n=0}^{N} roll(n), \tag{A.1}$$

$$roll_{std} = \sqrt{\frac{1}{N-1}\sum_{n=0}^{N}(roll(n) - \bar{roll}(n))^2}, \tag{A.2}$$

where N is the total sample size of the body roll angle $roll(n)$. Eqs. (A.1) and (A.2) show the mean and standard deviation of the roll angle during a locomotion period, respectively.

The standard deviation of the roll angle indicates amplitude oscillation during a period. Its inverse is defined as a stability metric as shown in Eq. (A.3). Thus, the larger the *stability* value, the higher the stable locomotion.

$$stability = \frac{1}{roll_{std}}. \tag{A.3}$$

Appendix D.2. Coordination

In addition to the body movement state, the robot foot motion also significantly determines locomotion performance. Here, we implement a symmetrical robot and control where each identical leg obtains its control commands with only a phase shift under a trot gait. Ideally, all robot feet should then be able to perform similar alternating movements from swing to stance. Thus, all legs should have the same duty factors while stably trotting. The coordination metric is used to measure the consistency of the duty factors, defined as:

$$\mu_i(m) = \frac{T^i_{swing}(m)}{T^i_{swing}(m) + T^i_{stance}(m)}, \tag{A.4}$$

$$\bar{\mu}(m) = \frac{1}{4}\sum_{i=1}^{4}(\mu_i(m)), \tag{A.5}$$

$$\mu_{std}(m) = \begin{cases} \sqrt{\dfrac{\sum_{i=1}^{4}(\mu_i(m) - \bar{\mu}(m))^2}{3}} & \forall m \le M, i \le 4, \exists \mu_i(m)\ , \\ 0 & \text{otherwise} \end{cases} \tag{A.6}$$

$$coordination = \begin{cases} \frac{1}{\max\limits_{\{m \in M\}} (\mu_{std}(m))} & \exists \mu_{std}(m) \neq 0 \\ 0 & \text{otherwise} \end{cases}, \quad \text{(A.7)}$$

where $T^i_{swing}(m)$ and $T^i_{stance}(m)$ in Eq. (A.4) are the swing and stance periods of the ith leg of the mth step, respectively. Thus, $\mu_i(m)$ defines the duty factor of the mth step of the ith leg, thereby the mean ($\bar{\mu(m)}$) and standard deviation ($\mu_{std}(m)$) of the duty factor for the four legs at the mth step are given to measure the irregularity/incongruity of the four leg movements. The inverse of the maximum standard deviation during several steps (i.e., M) is used to characterize the coordinated movement of the four legs. Therefore, the larger the *coordination* value, the greater the coordination in a regular trot gait.

Appendix D.3. Displacement

Displacement is a basic measurement of legged robot locomotion. Thus, we induce a metric *displacement*. It is defined as the locomotion displacement of the robots at a given period. It is defined as:

$$displacement = \sqrt{(x(N) - x(0))^2 + (y(N) - y(0))^2 + (z(N) - z(0)^2)}, \quad \text{(A.8)}$$

where x, y, and z are the distances along three directions in world coordinate, N indicates the total sample size.

Appendix E. Abbreviations and Acronyms

BBO = Black box optimization.
CPG(s) = Central pattern generator(s).
DFFB = Distributed force feedback-based
DFRL = Distributed force feedback-based reflex with online learning
DIL = Dual integral learner
GRF(s) = Ground reaction force(s).
LF = Left front leg.

LH = Left hind leg.

MN(s) = Motor neuron(s).

MPC = Model predictive control.

PI2 = Path integrals.

RF = Right front leg.

RH = Right hind leg.

RL = Reinforcement learning.

ROS = Robot operation system.

ZMP = Zero moment point.

Acknowledgment

The authors would like to thank Xiaofeng Xiong, Mathias Thor, Weijia Zong, Huijuan He and Chris Bang Sørense for providing fruitful discussions, and Song Xu and Yan Li for proofreading. We also gratefully acknowledge the financial support of the NUAA research fund (Grant No. 1005-YQRO7001, P.M., Project PI), NSFC-DFG Collaborative Research Program (Grant No. 51861135306, P.M., project Co-PI), the National Natural Science Foundation of China (Grant No. 51435008 to Z.D), and Chinese Government Scholarship (Grant No. CSC201906830012) [TS]).

References

[1] A. J. Ijspeert, Biorobotics: Using robots to emulate and investigate agile locomotion, science 346 (6206) (2014) 196–203.

[2] E. Ackerman, Boston dynamics spotmini is all electric, agile, and has a capable face-arm, IEEE SPECTRUM (2016).

[3] M. Hutter, C. Gehring, D. Jud, A. Lauber, C. D. Bellicoso, V. Tsounis, J. Hwangbo, K. Bodie, P. Fankhauser, M. Bloesch, et al., Anymal-a highly mobile and dynamic quadrupedal robot, in: 2016 IEEE/RSJ International

Conference on Intelligent Robots and Systems (IROS), IEEE, 2016, pp. 38–44.

[4] G. Bledt, M. J. Powell, B. Katz, J. Di Carlo, P. M. Wensing, S. Kim, Mit cheetah 3: Design and control of a robust, dynamic quadruped robot, in: 2018 IEEE/RSJ International Conference on Intelligent Robots and Systems (IROS), IEEE, 2018, pp. 2245–2252.

[5] M. Kalakrishnan, J. Buchli, P. Pastor, M. Mistry, S. Schaal, Learning, planning, and control for quadruped locomotion over challenging terrain, The International Journal of Robotics Research 30 (2) (2011) 236–258.

[6] C. Semini, V. Barasuol, J. Goldsmith, M. Frigerio, M. Focchi, Y. Gao, D. G. Caldwell, Design of the hydraulically actuated, torque-controlled quadruped robot hyq2max, IEEE/ASME Transactions on Mechatronics 22 (2) (2017) 635–646.

[7] M. Hutter, C. Gehring, A. Lauber, F. Gunther, C. D. Bellicoso, V. Tsounis, P. Fankhauser, R. Diethelm, S. Bachmann, M. Blösch, et al., Anymal-toward legged robots for harsh environments, Advanced Robotics 31 (17) (2017) 918–931.

[8] S. Fahmi, C. Mastalli, M. Focchi, C. Semini, Passive whole-body control for quadruped robots: Experimental validation over challenging terrain, IEEE Robotics and Automation Letters 4 (3) (2019) 2553–2560.

[9] J. Carlo, P. Wensing, B. Katz, G. Bledt, S. Kim, Dynamic locomotion in the mit cheetah 3 through convex model-predictive control, in: 2018 IEEE/RSJ International Conference on Intelligent Robots and Systems (IROS), 2018, pp. 1–9. doi:10.1109/IROS.2018.8594448.

[10] P. Manoonpong, U. Parlitz, F. Wrgtter, Neural control and adaptive neural forward models for insect-like, energy-efficient, and adaptable locomotion of walking machines, Frontiers in Neural Circuits 7 (2013) 12.

[11] A. J. Ijspeert, Central pattern generators for locomotion control in animals and robots: a review, Neural networks 21 (4) (2008) 642–653.

[12] J. H. Barron-Zambrano, C. Torres-Huitzil, Fpga implementation of a configurable neuromorphic cpg-based locomotion controller, Neural Networks 45 (2013) 50 – 61.

[13] M. R. Dimitrijevic, Y. Gerasimenko, M. M. Pinter, Evidence for a spinal central pattern generator in humans, Annals of the New York Academy of Sciences 860 (1) (1998) 360–376.

[14] E. Marder, D. Bucher, Central pattern generators and the control of rhythmic movements, Current biology 11 (23) (2001) R986–R996.

[15] M. MacKay-Lyons, Central pattern generation of locomotion: a review of the evidence, Physical therapy 82 (1) (2002) 69–83.

[16] A. J. Ijspeert, A. Crespi, D. Ryczko, J.-M. Cabelguen, From swimming to walking with a salamander robot driven by a spinal cord model, science 315 (5817) (2007) 1416–1420.

[17] Y. Fukuoka, H. Kimura, A. H. Cohen, Adaptive dynamic walking of a quadruped robot on irregular terrain based on biological concepts, The International Journal of Robotics Research 22 (3-4) (2003) 187–202.

[18] D. Owaki, T. Kano, K. Nagasawa, A. Tero, A. Ishiguro, Simple robot suggests physical interlimb communication is essential for quadruped walking, Journal of The Royal Society Interface 10 (78) (2013) 20120669.

[19] T. Sun, D. Shao, Z. Dai, P. Manoonpong, Adaptive neural control for self-organized locomotion and obstacle negotiation of quadruped robots, in: 2018 27th IEEE International Symposium on Robot and Human Interactive Communication (RO-MAN), IEEE, 2018, pp. 1081–1086.

[20] M. Thor, P. Manoonpong, Error-based learning mechanism for fast online adaptation in robot motor control, IEEE Transactions on Neural Networks and Learning Systems 31 (6) (2020) 2042–2051.

[21] K. Matsuoka, Mechanisms of frequency and pattern control in the neural rhythm generators, Biological cybernetics 56 (5-6) (1987) 345–353.

[22] D. T. Tran, I. M. Koo, Y. H. Lee, H. Moon, S. Park, J. C. Koo, H. R. Choi, Central pattern generator based reflexive control of quadruped walking robots using a recurrent neural network, Robotics and autonomous systems 62 (10) (2014) 1497–1516.

[23] C. Liu, L. Xia, C. Zhang, Q. Chen, Multi-layered cpg for adaptive walking of quadruped robots, Journal of Bionic Engineering 15 (2) (2018) 341–355.

[24] X. Zhang, H. Zheng, Walking up and down hill with a biologically-inspired postural reflex in a quadrupedal robot, Autonomous Robots 25 (1-2) (2008) 15–24.

[25] J. Sousa, V. Matos, C. P. dos Santos, A bio-inspired postural control for a quadruped robot: an attractor-based dynamics, in: 2010 IEEE/RSJ International Conference on Intelligent Robots and Systems, IEEE, 2010, pp. 5329–5334.

[26] M. Ajallooeian, S. Pouya, A. Sproewitz, A. J. Ijspeert, Central pattern generators augmented with virtual model control for quadruped rough terrain locomotion, in: 2013 IEEE international conference on robotics and automation, IEEE, 2013, pp. 3321–3328.

[27] T. Sun, X. Xiong, Z. Dai, P. Manoonpong, Small-sized reconfigurable quadruped robot with multiple sensory feedback for studying adaptive and versatile behaviors, Frontiers in Neurorobotics 14 (2020) 14.

[28] X. Zhao, J. Zhang, C. Qi, Cpg and reflexes combined adaptive walking control for aibo, in: 2012 11th International Conference on Machine Learning and Applications, Vol. 1, IEEE, 2012, pp. 448–453.

[29] D. V. Lee, Effects of grade and mass distribution on the mechanics of trotting in dogs, Journal of Experimental Biology 214 (3) (2011) 402–411.

[30] C. Gehring, C. D. Bellicoso, S. Coros, M. Bloesch, P. Fankhauser, M. Hutter, R. Siegwart, Dynamic trotting on slopes for quadrupedal robots, in: 2015 IEEE/RSJ International Conference on Intelligent Robots and Systems (IROS), IEEE, 2015, pp. 5129–5135.

[31] N. Heess, D. TB, S. Sriram, J. Lemmon, J. Merel, G. Wayne, Y. Tassa, T. Erez, Z. Wang, S. M. A. Eslami, M. Riedmiller, D. Silver, Emergence of locomotion behaviours in rich environments (2017). arXiv:1707.02286.

[32] J. Hwangbo, J. Lee, A. Dosovitskiy, D. Bellicoso, V. Tsounis, V. Koltun, M. Hutter, Learning agile and dynamic motor skills for legged robots, Science Robotics 4 (26) (2019). arXiv:https://robotics.sciencemag.org/content/4/26/eaau5872.full.pdf, doi:10.1126/scirobotics.aau5872.
URL https://robotics.sciencemag.org/content/4/26/eaau5872

[33] W. Jones, T. Blum, K. Yoshida, Adaptive slope locomotion with deep reinforcement learning, in: 2020 IEEE/SICE International Symposium on System Integration (SII), IEEE, 2020, pp. 546–550.

[34] T. Mathias, K. Tomas, M. Poramage, Generic neural locomotion control framework for legged robots (accepted), IEEE Transactions on Neural Networks and Learning Systems 2020 (2020).
URL https://mathiasthor.github.io/publications/

[35] Y. Nakamura, T. Mori, M. aki Sato, S. Ishii, Reinforcement learning for a biped robot based on a cpg-actor-critic method, Neural Networks 20 (6) (2007) 723 – 735. doi:https://doi.org/10.1016/j.neunet.2007.01.002.
URL http://www.sciencedirect.com/science/article/pii/S089360800700024X

[36] F. Pasemann, M. Hild, K. Zahedi, So (2)-networks as neural oscillators, in: International Work-Conference on Artificial Neural Networks, Springer, 2003, pp. 144–151.

[37] S. Tao, D. Zhendong, M. Poramate, Robust and reusable self-organized locomotion of legged robots under adaptive physical and neural communications (under review), IEEE transactions on Cybnertics (2020).
URL https://gitlab.com/neutron-nuaa/lilibot/-/wikis/Publication

[38] L. Righetti, J. Buchli, M. Mistry, M. Kalakrishnan, S. Schaal, Optimal distribution of contact forces with inverse-dynamics control, The International Journal of Robotics Research 32 (3) (2013) 280–298.

[39] Z. Li, S. S. Ge, S. Liu, Contact-force distribution optimization and control for quadruped robots using both gradient and adaptive neural networks, IEEE transactions on neural networks and learning systems 25 (8) (2013) 1460–1473.

[40] J. H. Lee, J. H. Park, Optimization of postural transition scheme for quadruped robots trotting on various surfaces, IEEE Access 7 (2019) 168126–168140.

[41] M. Vukobratović, B. Borovac, Zero-moment pointthirty five years of its life, International journal of humanoid robotics 1 (01) (2004) 157–173.

[42] C. Yu, L. Zhou, H. Qian, Y. Xu, Posture correction of quadruped robot for adaptive slope walking, in: 2018 IEEE International Conference on Robotics and Biomimetics (ROBIO), IEEE, 2018, pp. 1220–1225.

[43] M. Raibert, K. Blankespoor, G. Nelson, R. Playter, Bigdog, the rough-terrain quadruped robot, IFAC Proceedings Volumes 41 (2) (2008) 10822–10825.

[44] G. Urbain, V. Barasuol, C. Semini, J. Dambre, F. wyffels, Stance control inspired by cerebellum stabilizes reflex-based locomotion on hyq robot (2020). arXiv:2003.09327.

[45] G. E. Stutzmann, B. S. McEwen, J. E. LeDoux, Serotonin modulation of sensory inputs to the lateral amygdala: dependency on corticosterone, Journal of Neuroscience 18 (22) (1998) 9529–9538.

[46] T. Deemyad, M. G. Metzen, Y. Pan, M. J. Chacron, Serotonin selectively enhances perception and sensory neural responses to stimuli generated by same-sex conspecifics, Proceedings of the National Academy of Sciences 110 (48) (2013) 19609–19614.

[47] E. Lottem, M. L. Lörincz, Z. F. Mainen, Optogenetic activation of dorsal raphe serotonin neurons rapidly inhibits spontaneous but not odor-evoked activity in olfactory cortex, Journal of Neuroscience 36 (1) (2016) 7–18.

[48] M. C. Avery, J. L. Krichmar, Neuromodulatory systems and their interactions: A review of models, theories, and experiments, Frontiers in Neural Circuits 11 (2017) 108.

[49] U. Sawiska, L. M. Jordan, Serotonergic influences on locomotor circuits, Current Opinion in Physiology 8 (2019) 63 – 69.

[50] H. Kimura, Y. Fukuoka, A. H. Cohen, Adaptive dynamic walking of a quadruped robot on natural ground based on biological concepts, The International Journal of Robotics Research 26 (5) (2007) 475–490. doi:10.1177/0278364907078089.

[51] R. Hodoshima, T. Doi, Y. Fukuda, S. Hirose, T. Okamoto, J. Mori, Development of titan xi: a quadruped walking robot to work on slopes, in: 2004 IEEE/RSJ International Conference on Intelligent Robots and Systems (IROS)(IEEE Cat. No. 04CH37566), Vol. 1, IEEE, 2004, pp. 792–797.

[52] J. He, J. Shao, G. Sun, X. Shao, Survey of quadruped robots coping strategies in complex situations, Electronics 8 (12) (2019) 1414.

[53] D. J. Dutto, D. F. Hoyt, E. A. Cogger, S. J. Wickler, Ground reaction forces in horses trotting up an incline and on the level over a range of speeds, Journal of Experimental Biology 207 (20) (2004) 3507–3514.

[54] Y. N. G. Hong, J. Lee, C. S. Shin, Transition versus continuous slope walking: adaptation to change center of mass velocity in young men, Applied bionics and biomechanics 2018 (2018). doi:10.1155/2018/2028638.
URL https://doi.org/10.1155/2018/2028638

[55] Z.-Y. Wang, A.-H. Ji, T. Endlein, W. Li, D. Samuel, Z.-D. Dai, Locomotor kinematics of the gecko (tokay gecko) upon challenge with various inclines, Chinese science bulletin 59 (33) (2014) 4568–4577.

[56] M. Focchi, A. Del Prete, I. Havoutis, R. Featherstone, D. G. Caldwell, C. Semini, High-slope terrain locomotion for torque-controlled quadruped robots, Autonomous Robots 41 (1) (2017) 259–272.

[57] M. Iosa, T. Marro, S. Paolucci, D. Morelli, Stability and harmony of gait in children with cerebral palsy, Research in Developmental Disabilities 33 (1) (2012) 129–135.

[58] C. Ferreira, C. P. Santos, A sensory-driven controller for quadruped locomotion, Biological cybernetics 111 (1) (2017) 49–67.